University of Glasgow

Handley, H.K., Reagan, M., Gertisser, R., Preece, K., Berlo, K., McGee, L.E., Barclay, J. and Herd, R. (2018) Timescales of magma ascent and degassing and the role of crustal assimilation at Merapi volcano (2006-2010), Indonesia: constraints from uranium-series and radiogenic isotopic compositions. *Geochimica et Cosmochimica Acta*, 222, pp. 34-52. (doi:10.1016/j.gca.2017.10.015)

This is the author's final accepted version.

There may be differences between this version and the published version. You are advised to consult the publisher's version if you wish to cite from it.

http://eprints.gla.ac.uk/150854/

Deposited on: 30 October 2017

Enlighten – Research publications by members of the University of Glasgow
http://eprints.gla.ac.uk

For submission to Geochimica et Cosmochima Acta

Timescales of magma ascent and degassing and the role of crustal assimilation at Merapi volcano (2006-2010), Indonesia: constraints from uranium-series and radiogenic isotopic compositions

H. K. Handley[1*], M. Reagan[2], R. Gertisser[3], K. Preece[4,5], K. Berlo[6], L. E. McGee[1], J. Barclay[4], R. Herd[4]

[1]Department of Earth and Planetary Sciences, Macquarie University, Sydney, NSW 2109, Australia

[2] Department of Earth and Environmental Sciences, The University of Iowa, Iowa City, IA 52242, USA

[3]School of Geography, Geology and the Environment, Keele University, Keele, ST5 5BG, UK

[4]School of Environmental Sciences, University of East Anglia, Norwich, NR4 7TJ, UK

[5]Isotope Geoscience Unit, Scottish Universities Environmental Research Centre, East Kilbride, G75 0QF, UK

[6]Department of Earth and Planetary Sciences, McGill University, Montreal, H3A 0E8, Canada

Keywords: differentiation, explosive, petrogenesis, subduction zone, ^{238}U-^{230}Th-^{226}Ra-^{210}Pb-^{210}Po, Sr-Nd-Pb isotopes

*Corresponding author. Department of Earth and Planetary Sciences, Macquarie University, Sydney, NSW 2109 Australia. Telephone: +61 2 9850 4403. Fax: +61 2 9850 8943. Email: heather.handley@mq.edu.au

Abstract

We present new ^{238}U-^{230}Th-^{226}Ra-^{210}Pb-^{210}Po, $^{87}Sr/^{86}Sr$ and $^{143}Nd/^{144}Nd$ isotopic data of whole-rock samples and plagioclase separates from volcanic deposits of the 2006 and 2010 eruptions at Merapi volcano, Java, Indonesia. These data are combined with available eruption monitoring, petrographic, mineralogical and Pb isotopic data to assess current theories on the cause of a recent transition from effusive dome-building (2006) to explosive (2010) activity at the volcano, as well as to further investigate the petrogenetic components involved in magma genesis and evolution. Despite the significant difference in eruption style, the 2006 and 2010 volcanic rocks show no significant difference in ($^{238}U/^{232}Th$), ($^{230}Th/^{232}Th$) and ($^{226}Ra/^{230}Th$) activity ratios, with all samples displaying U and Ra excesses. The ^{226}Ra and ^{210}Pb excesses observed in plagioclase separates from the 2006 and 2010 eruptions indicate that a proportion of the plagioclase grew within the decades preceding eruption. The 2006 and 2010 samples were depleted in ^{210}Po relative to ^{210}Pb ($(^{210}Po/^{210}Pb)_i$ <1) at the time of eruption but were variably degassed (69% to 100%), with the degree of ^{210}Pb degassing strongly related to sample texture and eruption phase. In good agreement with several activity monitoring parameters, ^{210}Po ingrowth calculations suggest that initial intrusion into the shallow magma plumbing system occurred several weeks to a few months prior to the initial 2010 eruption. The 2006 and 2010 samples show a wide range in ($^{210}Pb/^{226}Ra$) activity ratio within a single eruption at Merapi and are largely characterised by ^{210}Pb deficits (($^{210}Pb/^{226}Ra$) <1). Assuming a model of complete radon degassing, the ^{210}Pb deficits in the 2006 volcanic rocks indicate relatively longer degassing timescales of ~2-4 years than those given by the 2010 samples of ~0-3 years. The uranium-series and radiogenic isotopic data do not support greater crustal assimilation of carbonate material as the explanation for the more explosive behaviour of Merapi in 2010 (as has been previously suggested) and instead indicate that relatively rapid ascent of a more undegassed magma was the primary difference responsible for the transition in explosive behaviour. This interpretation is in good agreement with gas monitoring data, previous petrological studies (mineral, microlite and melt inclusion work) and maximum calculated timescale estimates using Fe-Mg compositional gradients in clinopyroxene, that also suggest more rapid movement of relatively undegassed magma in 2010 relative to 2006.

1. Introduction

Many volcanoes undergo relatively rapid changes in eruption explosivity, often exhibiting transitions between effusive and explosive behaviour both within and between eruptions,

such as at Soufriere Hills Volcano, Lesser Antilles (e.g., Edmonds and Herd, 2007), Novarupta, Alaska (e.g., Nguyen et al., 2014) Kelut, Indonesia (e.g., Jeffery et al., 2013) and Volcán de Colima, Mexico (e.g., Zobin et al., 2015). Therefore understanding the drivers of such change is of great importance for volcanic hazard mitigation.

Merapi Volcano, located 25 km north of Yogyakarta in Central Java in the Sunda arc, is one of the most active volcanoes in Indonesia. The 2010 explosive eruption was the volcano's largest eruption since 1872, resulted in the highest number of fatalities since the 1930 eruption and was much more violent than expected. Prior to the 2010 eruption, recent volcanic activity at Merapi was characterised by the growth and collapse of lava domes (e.g., Andreastuti et al., 2000; Camus et al., 2000; Newhall et al., 2000; Voight et al., 2000; Gertisser et al., 2012), for example, as witnessed in 2006 (Charbonnier and Gertisser, 2008; 2011; Preece et al., 2013; Ratdomopurbo et al., 2013). Whether eruptions at Merapi are effusive or explosive in character is thought to result from a number of factors, such as variations in magma supply from depth, magma ascent rate, magma degassing behaviour and the assimilation of crustal carbonates (Newhall et al., 2000; Gertisser and Keller, 2003a; Chadwick et al., 2007; Deegan et al. 2010; Surono et al., 2012; Troll et al., 2012; 2013; Borisova et al., 2013; 2016; Costa et al., 2013; Preece et al., 2013; 2014; 2016). Petrologic and monitoring data suggest the rapid ascent of a significantly larger, volatile-rich (i.e. relatively undegassed) magma body, and its possible interaction with crustal carbonates, caused the significant change in explosive behaviour of the volcano between 2006 and 2010 (Surono et al., 2012; Borisova et al., 2013; Costa et al., 2013; Preece et al., 2013; 2014; 2016; Erdmann et al., 2016).

The uranium-series (U-series) nuclides provide unique timescale information on magmatic processes ranging from melt production, differentiation and ascent to magmatic degassing prior to eruption (e.g., Bennett et al., 1982; Gill and Williams, 1990; Turner et al., 2000; Condomines et al., 2003; Peate and Hawkesworth 2005; Bourdon et al., 2006; Reagan et al., 2006; Handley et al., 2008; Reagan et al., 2008; Berlo et al., 2010; Sims et al., 2013; Bragagni et al., 2014) as the nuclides have varied geochemical properties that cause them to be fractionated in distinct ways by different magmatic processes (see Peate and Hawkesworth (2005) for a review). At secular equilibrium the activities of the nuclides (denoted by parentheses) are equal, for example, $(^{230}Th/^{238}U) = 1$. If the decay chain is affected by chemical fractionation of a parent/daughter elemental ratio, restoration of equilibrium by radioactive decay is determined by the half-life of the daughter nuclide involved. Excess ^{238}U $((^{238}U/^{230}Th)>1)$ and ^{226}Ra $((^{226}Ra/^{230}Th) >1)$ in subduction zone volcanic rocks are typically

attributed to fluid addition from the subduction slab on timescales of less than ~380,000 years and less than ~8,000 years, respectively (e.g., Condomines et al., 1988; Gill and Williams, 1990; Hawkesworth et al., 1997) although there may be some modification of ratios by crustal-level processes (e.g., Handley et al., 2008; Reubi et al., 2014; Huang et al., 2016). At magmatic temperatures, ^{234}U is not expected to be fractionated from ^{238}U, and so fresh igneous rocks should have $(^{234}U/^{238}U) = 1$.

Detailed studies of the shorter-lived U-series nuclides from individual volcanic centres, for example, ^{210}Po (half-life = 138.4 days) and its 'grandparent' ^{210}Pb (half-life = 22.6 years), require the collection of young, fresh and dated samples that need to be analysed within a short timeframe after eruption. Polonium partitions efficiently into exsolving volatile phases and is almost completely lost during eruption (Bennett et al., 1982; Gill et al., 1985, Rubin and Macdougall, 1989; Reagan et al., 2008), which results in $(^{210}Po/^{210}Pb) << 1.0$ in erupted lavas. The short-lived ^{210}Pb nuclide is produced by decay of the gas ^{222}Rn (half-life = 3.8 days), which readily enters the volatile phase in magmas (Lambert et al., 1985; Gill et al., 1985). Persistent loss or gain of ^{222}Rn via magmatic degassing or volatile accumulation will therefore create disequilibrium between the nuclides situated before and after ^{222}Rn, that is between the parent ^{226}Ra and the daughter ^{210}Pb. As a result, in an open, degassing system where ^{222}Rn is efficiently lost in the gas phase, deficits of ^{210}Pb are expected, i.e. $(^{210}Pb/^{226}Ra) < 1$. Thus, ^{210}Pb deficits can constrain the duration of degassing (e.g., Gauthier and Condomines, 1999). Alternatively, if gas is supplied from underlying fresh (and probably more mafic) magma, it is possible to create a ^{210}Pb excess (e.g., Kayzar et al., 2009; Condomines et al., 2010).

Previous ^{210}Pb-^{226}Ra disequilibria measurements on Merapi volcanic rocks erupted between 1981-1995 showed variable initial $(^{210}Pb/^{226}Ra)$ ratios, from 0.75 to 1 (Gauthier and Condomines, 1999). Based on these data, a <10-year cycle of closed-system magmatic evolution with open degassing followed by episodes of undegassed magmatic recharge was proposed for Merapi (Gauthier and Condomines, 1999). In a study of (^{210}Pb), (^{210}Bi), and (^{210}Po) activities and SO_2 in Merapi gaseous emissions conducted between 1978–1995, it was found that growing dome magma had been completely degassed when it reached the surface. It was also suggested that the non-explosive (dome-building) eruptions arise due to open-system degassing at depth beneath the volcano (Le Cloarec and Gauthier, 2003).

Abundant, young volcanic samples from progressive phases of the dome-forming eruption in 2006 and the highly explosive eruption in 2010 at Merapi volcano, provide a rare opportunity to conduct a detailed ^{210}Po-^{210}Pb-^{226}Ra disequilibria study and provide insight

from ^{238}U-^{230}Th-^{226}Ra-^{210}Pb-^{210}Po disequilibria and Sr-Nd-Pb isotopic compositions on magmatic source components, the role of assimilation of carbonate material and the timescales of magmatic degassing. The data are used to assess current theories on the recent transition from effusive to explosive eruption at Merapi (e.g., Surono et al., 2012; Borisova et al., 2013; 2016; Costa et al., 2013; Preece et al., 2013; 2014; 2016; Erdmann et al., 2016) and to further investigate the proposed periodicity in magmatic degassing and recharge at Merapi (Gauthier and Condomines, 1999) over a longer time period, ending with the cataclysmic eruption in 2010.

2. Summary of the 2006 and 2010 volcanic eruptions of Merapi

Over the last two centuries, dominant volcanic activity at Merapi has characteristically consisted of the growth and collapse of basaltic-andesite lava domes, producing relatively small-volume pyroclastic density currents (PDCs) on a periodicity of 4-6 years, with larger explosive eruptions recurring on the order of centuries (Andreastuti et al., 2000; Camus et al., 2000; Newhall et al, 2000; Voight et al., 2000; Gertisser et al., 2012).

The April to October 2006 eruption (Volcanic Explosivity Index (VEI) 1) was characterised by typical recent Merapi activity, with episodes of lava dome growth and collapse. Early eruption seismic precursors suggest that the first signs of new activity were detected by seismic and deformation data in July 2005, which increased from December 2005 to mid-April 2006 (Ratdomopurbo et al., 2013). The full chronology of events of the 2006 eruption can be found in Charbonnier and Gertisser (2008; 2011), Preece et al. (2013) and Ratdomopurbo et al. (2013). Lava dome extrusion likely began between 26-28 April 2006 and continued throughout May, with the first dome collapses on 11 May, producing PDCs extending less than 4 km from the summit to the southwest. Three major collapse stages took place from 4 to 14 June (Charbonnier and Gertisser, 2008, 2011; Ratdomopurbo et al., 2013) destroying most of the dome and forming a series of PDCs that reached up to 7 km from the summit at the peak of activity on 14 June (Charbonnier and Gertisser, 2008, 2011; Lube et al., 2011; Ratdomopurbo et al., 2013). A new lava dome was observed inside the new crater on 26 June, which continued to grow until October 2006 (Preece et al., 2013; Ratdomopurbo et al., 2013).

In contrast, the following October-November 2010 eruption (VEI 4) at Merapi was the largest eruption since 1872 (Surono et al., 2012). After approximately one year of unrest and intrusion (Stage 1; 31 October 2009 to 25 October 2010), initial phreatomagmatic explosions occurred between 26 and 29 October (Stage 2) (Komorowski et al., 2013),

followed by recurrent rapid dome growth and destruction during 29 October to 4 November (Stage 3). Dome extrusion rates in 2010 were extremely rapid at >25 m^3s^{-1} on average (Pallister et al., 2013) compared to 1 to 4 $m^3 s^{-1}$ for the 2006 eruption (Ratdomopurbo et al., 2013). A series of laterally-directed explosions (Stage 4) and retrogressive dome collapses (Stage 5) occurred during the climactic eruption phase on 5 November. These produced valley-confined, concentrated pyroclastic density currents that travelled up to ~16 km from the summit, and contemporaneous widespread, high-energy pyroclastic density currents. Sulphur dioxide emission levels also peaked at this time (Surono et al., 2012; Fig. 1). Following a sub-Plinain phase and fountain collapse (Stage 6), further dome growth and multiple ash plumes continued until 8 November (Stage 7). The activity waned towards the end of November (Stage 8), with decreasing intensity of gas and ash emissions (e.g., Surono et al., 2012; Charbonnier et al., 2013; Cronin et al., 2013; Komorowski et al., 2013; Preece et al., 2014; 2016). Detailed chronological accounts of the eruption (noting slight discrepancies in eruption timings between accounts) are presented in Surono et al. (2012), Charbonnier et al. (2013), Cronin et al. (2013), Komorowski et al. (2013) and Preece et al. (2014). The estimated deposit (non-DRE) volume for the 2010 eruption of ~ 30-60 x 10^6 m^3 (Surono et al., 2012; Charbonnier et al., 2013) is also much greater than that for the 2006 eruption at ~8.7 x 10^6 m^3 (Charbonnier and Gertisser, 2011). In the months preceding the 2010 eruption, a significant increase in CO_2 abundance (10 wt% to 35-63 wt% from September to 20 October) and CO_2/SO_2, CO_2/HCl and CO_2/H_2O ratios suggested a progressive shift to a deep degassing source (Surono et al., 2012), which has been corroborated by petrological studies (Costa et al., 2013; Preece et al., 2014; 2016). Time-series of SO_2 flux estimated from ground-DOAS and satellite measurements show that the SO_2 emission rates during the 2010 eruption were orders of magnitude higher than during the previous eruption period in 2006 (Fig. 1) and were correlated with energetic tremor and high eruption rates during the most explosive phases of the eruption (Surono et al., 2012). High SO_2 emissions accompanied the initial explosive eruptions on 26 October and again between 29-30 October 2010. The emissions then decreased during the extrusion and growth of a lava dome and peaked during the climatic phase of the eruption on 5 November (Surono et al., 2012) (Fig. 1).

Juvenile material erupted in both 2006 and 2010 displays similar whole-rock compositions of ~55-56 wt% SiO_2 (Surono et al., 2012; Costa et al., 2013; Preece et al., 2013; 2014; 2016) and similar mineral assemblages dominated by plagioclase with clinopyroxene, orthopyroxene and minor amphibole and titanomagnetite. However, most amphibole phenocrysts in the juvenile 2010 material do not show reaction rims, whereas

many within the 2006 deposits are largely reacted (Surono et al., 2012; Costa et al., 2013; Preece at al., 2013, 2014). The lack of amphibole reaction rims in 2010 deposits along with microlite textural and compositional analysis, suggest minimal storage and relatively rapid movement of the 2010 magma relative to that erupted in 2006 (Preece et al., 2013; 2014; 2016).

3. Samples and analytical procedures

A summary of the sample textural types selected for U-series isotopic analysis is given in Tables 1 and 2. A detailed description of samples (except MER061406-L and MER061406-D) can be found in Preece (2014) and Preece et al. (2013; 2014; 2016). Samples MER061406-L and MER061406-D are scoriaceous fragments collected from a PDC deposit erupted 14 June, 2006. The "L" sample is light grey, highly crystalline and has ~30% vesicles. The sample contains about 30% plagioclase (<1.3 mm in length), 5% clinopyroxene (<0.7 mm), 3% magnetite (<0.2 mm), and < 1% hornblende (<1 mm) and orthopyroxene (<0.3 mm). Plagioclase is euhedral, complexly zoned and typically has abundant inclusions of glass, magnetite, and clinopyroxene. Clinopyroxene also is euhedral with abundant inclusions of magnetite and apatite. Hornblende is anhedral with variably thick reaction rims of plagioclase, orthopyroxene, magnetite, and clinopyroxene. Orthopyroxene is anhedral with optically continuous clinopyroxene rims. The remaining approximately 30% is groundmass consisting of glass, plagioclase, magnetite, orthopyroxene, and clinopyroxene. The "D" (dark grey-brown) sample is similarly vesicular and highly crystalline, but has a more mafic mineral assemblage of ~40% complexly zoned plagioclase (< 1 mm), 10% clinopyroxene (< 1mm), 3% magnetite (<0.1 mm), and < 1% olivine (<1 mm). The olivine is anhedral with ~0.1 mm reaction rims of granular clinopyroxene. The groundmass in this sample is finely holocrystalline, mostly plagioclase and partially oxidized magnetite.

The relationship of samples to the eruption chronology is given in Table 1 and follows that presented in Preece et al. (2013) for the 2006 eruption, and Komorowski et al. (2013) and Preece et al. (2014; 2016) for the 2010 eruption. The light grey dense inclusions (LGD-Inc) are found as abundant angular inclusions ranging from millimetres to centimetres in size within the juvenile dome material. Occasionally, this lithology forms diffuse bands through the darker dome material and large, sometimes prismatically-jointed blocks (up to several metres in diameter) of this material have been found loose within the 2010 Stage 4 PDC deposits (Preece et al., 2016). There is some degree of uncertainty in the exact extrusion age of juvenile dense clasts from pyroclastic density current deposits, as for example, for the

2010 eruption, the juvenile dome material that collapsed on the 5 November was extruded anytime between 29 October and 4 November (see Table 1 footnote for further details on assumed eruptive age). However for the (^{210}Po) activities (which would be most affected by assumptions in extrusion age), whether the 29 October or 4 November is selected as the extrusion age, the calculated initial (^{210}Po) activities lie within 2σ error of each other.

Fresh samples MER061406-L and MER061406-D were ultrasonically washed in purified water, dried, reduced in a jaw crusher, and ground to powder in a ceramic mill. All other samples had any weathered edges removed prior to washing in deionized water, drying and processing to powder in an agate mill (Preece et al., 2013; Preece 2014). U, Th and Ra concentrations and isotopic ratios were determined on bulk-rock powders and plagioclase separates using the procedure employed by the Uranium-series Research Laboratory at Macquarie University GeoAnalytical (MQGA) for volcanic rock samples. Approximately 0.5 g of bulk-rock powder or 2 g of plagioclase separate was spiked with ^{236}U-^{229}Th and ^{228}Ra tracers and digested in a mixture of concentrated acids (HF-HNO_3-HCl). Separation of U and Th followed standard anionic resin chromatography as described in Turner et al. (2011). Uranium and thorium concentrations, determined by isotope dilution, and U-Th isotopic ratios were measured on a Nu Instrument Multi-Collector inductively coupled plasma mass spectrometer (MC-ICP-MS) at Macquarie University following the approach given by Turner et al. (2011). In addition, the New Brunswick Laboratory (NBL) U010 synthetic standard was used to carry out linear drift correction and normalisation of samples for U isotopes, using the certified atomic ratios of 5.47×10^{-5}, 1.01×10^{-2} and 6.88×10^{-5} for ^{234}U/^{238}U, ^{235}U/^{238}U and ^{236}U/^{238}U, respectively. The NBL synthetic standard U005-A was run as an unknown at regular intervals throughout the analytical session to assess the robustness of instrumental corrections. The average corrected U005-A ^{234}U/^{238}U, ^{235}U/^{238}U and ^{236}U/^{238}U ratios (n = 8) were $3.42 \pm 0.01 \times 10^{-5}$ (2SD), $5.09 \pm 0.01 \times 10^{-3}$ (2SD) and $1.18 \pm 0.01 \times 10^{-5}$ (2SD), which are within error of the NBL published values of 3.42×10^{-5}, 5.09×10^{-3} and 1.19×10^{-5}. Similarly, the UCSC Th 'A' was used as a monitor of the robustness of instrumental corrections during the analytical session. The average corrected Th 'A' (using the Th 'U' bracketing method detailed in Turner et al., 2011) ^{230}Th/^{232}Th ratio was $5.83 \times 10^{-6} \pm 0.04 \times 10^{-6}$ (2SD, n = 7), which is within error of the recommended ratio of 5.86×10^{-6} given by Sims et al. (2008) taken from Rubin (2001). The Table Mountain Latite (TML) rock standard, was digested and fully processed alongside the samples in each batch (n = 2) and the data are presented in Table 1. The (^{238}U/^{232}Th), (^{230}Th/^{232}Th) analyses of TML lie within error of

published values (e.g. Sims et al., 2008; Sims et al., 2013). However, the (^{230}Th/^{238}U) deviates by 2.5% from equilibrium. It is possible that due to the corrections required for MC-ICP-MS data (e.g., instrumental fractionation, ^{232}Th-tailing corrections and the uncertainties on half-lives) compared to measurements by alpha-spectrometry, that ^{230}Th is slightly underestimated for our samples. Nevertheless, there is no significant difference in U-Th isotopic ratios of the 2006 and 2010 rocks (Fig. 2). Replicate analysis of M11-05 and M07-53P gave (^{234}U/^{238}U), (^{238}U/^{232}Th), (^{230}Th/^{232}Th) and (^{238}U/^{230}Th) activity ratios within error of the initial analyses (Table 1). The Ra separation and analysis procedure follows that described by Turner et al. (2000; 2011). Samples were loaded onto degassed single Re filaments using a Ta-HF-H_3PO_4 activator solution (Birck, 1986) and ^{228}Ra/^{226}Ra ratios were measured in dynamic ion counting mode on a ThermoFinnigan Triton TIMS at Macquarie University. Accuracy was assessed via analysis of TML that yielded ^{226}Ra = 3594 fg/g and (^{226}Ra/^{230}Th) = 1.005 ± 0.008 (2SE), within internal analytical error of secular equilibrium. The Merapi (^{230}Th/^{232}Th) and (^{226}Ra/^{230}Th) ratios have not been recalculated for differences in eruption age as samples were analysed within 10 years of eruption and therefore, post-eruption radioactive decay is insignificant compared to the half-life of ^{230}Th (75,690 years) and ^{226}Ra (1599 years).

Analyses of ^{210}Po by alpha counting were performed at the University of Iowa, using methods described by Reagan et al. (2005; 2006) and Waters et al. (2013). Approximately 2 grams of whole rock powder or 3 grams of separated plagioclase were used for each ^{210}Po analysis. All whole rock powders with ages of less than two years and the plagioclase mineral separate were leached for 5 minutes in cold 0.5 N HCl using an ultrasonic agitator and triply washed in purified water. Older samples were ultrasonically washed in purified water. Samples and some supernates were spiked with a ^{209}Po solution calibrated against the TML standard and monitored with repeat analysis of RGM-2. The samples were subsequently digested using an HF-HNO_3 method, dried, dissolved in 1N HCl, and the solution passed through anion exchange resin to separate Po. Polonium was washed off the resin in warm 7.5 N HNO_3. The separated Po was autoplated on Ag in 0.5 N HCl and counted using an EGG Ortec alpha spectrometer. The 1995 sample and most 2006 samples were more than two years old at the time of measurement, i.e. five times the half-life of ^{210}Po (138.4 days) and therefore, (^{210}Pb) was considered equal to (^{210}Po). For the 2006 and 2010 samples repeatedly analysed soon (< 2 years) after eruption, the initial ^{210}Pb activities, $(^{210}Pb)_i$, representing ^{210}Pb activity at the time of eruption, and associated uncertainties were obtained through a Markov

Chain Monte Carlo simulation using Matlab. Only best-fitting models that fitted the data within analytical uncertainties were considered in the computation.

Samples for Sr and Nd isotopic analysis (from the same sample digestion as for U-Th isotopes) were prepared and analysed at the MQGA at Macquarie University. Sr and REE fractions were separated using a cationic column containing Biorad® AG50W-X8 (200-400 mesh) cationic exchange resin, after which Sm and Nd were separated using EIChrom® LN-spec resin following the column procedure given by Pin et al. (1997). Samples were loaded on to out-gassed single (Sr) and double (Nd) rhenium filaments using 2 µl of $TaCl_5$ + HF + H_3PO_4 + H_2O_2 and 5 µl of 1N HCl: 0.35N H_3PO_4 activator solutions, respectively. Analyses were performed in static mode on a ThermoFinnigan Triton® TIMS in the MQGA. Instrument mass fractionation was accounted for by normalizing $^{87}Sr/^{86}Sr$ and $^{143}Nd/^{144}Nd$ to $^{87}Sr/^{86}Sr = 0.1194$ and $^{143}Nd/^{144}Nd = 0.7219$, respectively. Sr and Nd blanks were lower than 1000 and 80 pg, respectively. Analysis of NIST SRM-987 gave 0.710214 ± 8 (2SE) and the JMC Nd standard gave 0.511116 ± 8 (2SE).

4. Results

4.1. ^{238}U-^{230}Th-^{226}Ra disequilibria in whole-rock samples and plagioclase

The new 2006 and 2010 Merapi whole-rock samples and plagioclase separates have U excesses (($^{238}U/^{230}Th$) activity ratios > 1) (Table 1, Fig. 2a), typical of subduction-related volcanic rocks. The 2010 samples show slightly greater variation in ($^{238}U/^{232}Th$) and ($^{230}Th/^{232}Th$) compared to the 2006 samples, although the data for both eruptions largely overlap. The new data in this study overlap with but display slightly lower ($^{230}Th/^{232}Th$) compared to the previously published, whole-rock Merapi data (Fig. 2a), which were largely produced by alpha spectrometry.

The 2006 and 2010 Merapi whole-rock samples and plagioclase separates have excess radium (($^{226}Ra/^{230}Th$) > 1) (Table 1, Fig. 2b) with no significant difference between the 2006 and 2010 whole-rock samples, and the majority of ($^{226}Ra/^{230}Th$) ratios lying between 3.0-3.3. The plagioclase separates also show similar ($^{226}Ra/^{230}Th$) ratios between the two eruptions of 3.5-3.7. The previously published historical and recent, whole-rock Merapi data (Gill and Williams, 1990; Gauthier and Condomines, 1999; Condomines et al., 2005) show comparable excess Ra values to the 2006 and 2010 samples (Fig. 2b).

4.2 ^{210}Po-^{210}Pb-^{226}Ra disequilibria

Repeated analysis of (^{210}Po) in leached, whole-rock material of two 2006 samples and the 2010 samples, all collected shortly after eruption, was carried out to constrain the initial ^{210}Po activity at the time of eruption (Table 2), i.e. where the growth curve intersects the y-axis at zero days since eruption in Fig. 3. The repeated sample measurements lie within analytical error of a single growth curve apart from sample MER061406-D, which has a high initial ^{210}Po activity of 2.95 dpm/g (Table 2; Fig. 3) and is therefore, not a juvenile fragment of the 2006 eruption. Excluding MER061406-D, the results show that the 2006 and 2010 samples were all depleted in ^{210}Po relative to ^{210}Pb ((^{210}Po/^{210}Pb)$_i$ < 1) at the time of eruption but were variably degassed (Table 2). The 2006 sample, MER061406-L, was 93% degassed on eruption with an initial (^{210}Po) of 0.21 (Table 2). For the 2010 samples, the pre-Nov 5 scoria (S2S; M11-28a) and light grey dense inclusion (LGD-Inc; M11-28b) samples erupted at the beginning of the eruptive period (26 October, Stage 2 of Komorowski et al., 2013), display intermediate initial (^{210}Po) compared to the other 2010 samples. The scoria sample has a lower initial (^{210}Po) compared to the LGD-Inc sample and is also relatively more degassed on eruption (87% compared to 74%). The dark dense, lava dome (DD) samples (M11-27-5 and M11-12) extruded during stage 3, i.e., the dome extrusion phase between 29 October and 4 November (Komorowski et al., 2013; Table 2) and emplaced in PDCs during stage 4 (labelled 1 Nov in Fig. 3) show the lowest initial (^{210}Po) and are 97% to 100% degassed of ^{210}Po at the time of eruption, which contrasts to the light grey inclusion (LGD-Inc; M11-05) from the same stage (Table 2). The LGD-Inc shows the highest initial (^{210}Po) and was 69% degassed of ^{210}Po at the time of eruption ((^{210}Po/^{210}Pb)$_i$ = 0.31, Table 2). The white pumice (WP; M11-18) erupted during sub-plinian fountaining on 5 November (Stage 6 of Komorowski et al., 2013) was 83% degassed of ^{210}Po at the time of eruption (Table 2).

The majority of the 2006 Merapi volcanic rocks were analysed several years post-eruption and therefore, due to the short half-life of ^{210}Po (138.4 days), the measured (^{210}Po) equates to the initial (^{210}Pb) at measurement date for these samples. The range in initial (^{210}Pb) activities for the 2006 samples analysed more than 2 years post-eruption (2.57-3.15 dpm/g, Table 2), are shown plotted along the right-hand y-axis in Fig. 3 and lie within the range displayed by the 2010 samples and sample MER061406-L from 2006 (comparing with the (^{210}Po) activities from the growth curves at ~800 days). The initial (^{210}Pb) activities determined from best-fit growth curves are relatively similar for the samples erupted in the middle stage of the 2010 eruption (2.93-3.13 dpm/g) but higher than those determined for the samples erupted earlier, on 26 October, in Stage 2 (2.38-2.64 dpm/g) (Table 2).

The initial $(^{210}Pb/^{226}Ra)_0$ activity ratios, calculated to the time of eruption, of the 2006 and 2010 Merapi volcanic rocks are presented in Table 2 and Fig. 1. The variation observed in $(^{210}Pb/^{226}Ra)_0$ for each of the 2006 and 2010 eruptions is comparable to the full range of ratios measured in the time period from 1981 to 1995, previously reported by Gauthier and Condomines (1999). With the exception of one DD 2010 sample (M11-27-5), the 2006 and 2010 samples are largely characterised by ^{210}Pb deficits ($(^{210}Pb/^{226}Ra)_0 < 1$), though four of the samples lie within error of secular equilibrium. Figs. 1b and c show $(^{210}Pb/^{226}Ra)_0$ ratios during different stages of the 2006 and 2010 eruptions, respectively. The 2006 samples show very little variation throughout the eruption, with most samples showing ^{210}Pb deficits. The sample erupted towards the end of the eruptive period lies within error of secular equilibrium. For the 2010 rocks, the LGD-Inc sample (M11-28b), representing the onset of the 2010 eruption (26 October; Stage 2) shows a significant ^{210}Pb deficit ($(^{210}Pb/^{226}Ra)_0$ of 0.79). This is followed by a change to near equilibrium ($^{210}Pb/^{226}Ra$) values for the LGD-Inc and DD samples extruded during the rapid dome growth and destruction period between the 29 October to 4 November (Stage 3) and emplaced in Stage 4. The white pumice sample erupted during the latest stages of the climactic phase of 5 November (Stage 6) lies within error of the Stage 4 emplaced samples with a ^{210}Pb deficit of 0.92. The 2010 plagioclase separate from a DD clast, M11-01P, has excess $(^{210}Pb)_i$ with $(^{210}Pb/^{226}Ra)_0 = 1.97 \pm 0.42$ (Table 2).

4.3. Sr-Nd-Pb radiogenic isotopes

Sr-Nd isotopic ratios have also been determined for selected 2006 and 2010 whole-rock samples and are presented in Table 3 and Fig. 4. The accompanying Pb isotope data are published in Handley et al. (2014) and presented in the inset to Fig. 4a. The $^{87}Sr/^{86}Sr$ and $^{143}Nd/^{144}Nd$ ratios of the 2006 and 2010 samples overlap and lie within the field of previously published data on historically erupted samples from the volcano (Woodhead et al., 2001; Gertisser and Keller, 2003a; Debaille et al., 2006), towards the higher $^{87}Sr/^{86}Sr$, low-intermediate $^{143}Nd/^{144}Nd$-end of the Merapi array, characteristic of the Merapi high-K series volcanic rocks that have erupted since ~1900 ^{14}C years B.P. (Gertisser et al., 2003a) (Fig. 4a). The 2006 and 2010 Pb isotope ratios are indistinguishable from one another and are remarkably similar to Pb isotope ratios determined for both high-K (<1900 ^{14}C yr B.P.) and medium-K (>1900 ^{14}C yr B.P.) Merapi volcanic rocks (Handley et al., 2014) (Table 3; Fig. 4a inset). The 2006, 2010 and previously published Merapi data plot within the range of Th isotopic ratios of other Javanese volcanic rocks (Turner and Foden, 2001) at slightly higher Sr isotopic composition (Fig. 4b). Local Javanese calcareous crustal samples (Gertisser and

Keller, 2003a; Gardner et al., 2012; Handley et al., 2014; Fig. 2 caption), a Merapi calc-silicate xenolith sample (Gertisser and Keller, 2003a), I-type Sumatran Granitoids (Gasparon and Varne, 1995) and altered oceanic crust (AOC; Staudigel et al., 1995) have similar Sr isotopic ratios to the Merapi samples but moderate to significantly higher estimated Th isotopic ratios. The Merapi samples have generally higher Th and lower Sr isotopic ratios compared to Indian Ocean pelagic sediments (Ben Othman et al., 1998; Gasparon and Varne, 1998), Bulk Java Sediment (Plank and Langmuir, 1998) and the two S-type Sumatran granites, with low Th and high Sr isotopic ratios (Gasparon and Varne, 1995). No correlations are observed between U-series activity ratios and Sr-Nd isotope ratios for the 2006 and 2010 samples (e.g., Fig 4b).

5. Discussion

As noted in Sections 1 and 2, previous studies of the 2010 Merapi volcanic rocks suggested that rapid ascent of a larger volume of more volatile-rich magma, with the additional potential contribution of CO_2 from the assimilation of carbonate crust was responsible for the more explosive eruption in 2010 compared to 2006 (Surono et al., 2012; Borisova et al., 2013; Costa et al., 2013; Preece et al., 2013; 2014; 2016; Erdmann et al., 2016). These hypotheses can be scrutinised and assessed with the new isotopic data.

5.1. Petrogenetic components and timescales of magmatic processes from U-Th-Ra disequilibria and radiogenic isotopic compositions

The 2006 and 2010 Merapi volcanic rocks are characterised by ^{238}U excesses (Fig. 2a), typical of subduction-related volcanic rocks, suggesting that recent fluid addition, likely from the down-going slab (e.g., Condomines et al., 1988; Gill and Williams, 1990; Hawkesworth et al., 1997) or that in-growth melting in the mantle and subsequent crustal modification (e.g., Reubi et al., 2014; Huang et al., 2016), occurred in the last 380 ka. In the past, Th isotopic variation in volcanic rocks (the vertical spread in data on the U-Th equiline diagram) has been used to estimate magma residence or storage times assuming closed-system differentiation (e.g., Heath et al., 1998). However, given the strong evidence for open-system processes, such as magmatic recharge and carbonate assimilation at Merapi volcano (e.g., Chadwick et al., 2007; Deegan et al., 2010; Borisova et al., 2013; Troll et al., 2013) and Merapi's almost continuous eruptive activity over the past few hundred years (Voight et al., 2000), the limited variation observed in ($^{230}Th/^{232}Th$) ratios in Fig. 2a is likely explained through the combination of magmatic differentiation, magma recharge and the potential

assimilation of carbonate material, instead of being attributed to a single process such as closed-system magmatic differentiation (see arrows in Fig. 2a).

Crustal assimilation of carbonate material is implicated in petrogenesis at Merapi (e.g., Chadwick et al., 2007, Deegan et al., 2010, Borisova et al., 2013; Troll et al., 2013) and has been proposed by some to play a role in the more explosive behaviour of the 2010 eruption (e.g., Borisova et al., 2013; 2016; Troll et al., 2013). A study by Allard et al. (1983) and more recent studies (e.g., Troll et al., 2012) on the $\delta^{13}C$ composition of fumarole gases from Merapi suggest that a high $\delta^{13}C$, non-magmatic CO_2 input may be important, such as that associated with late-stage crustal decarbonation reactions through assimilation of limestone and skarnification processes. Javanese limestone or calcareous marl is expected to have a higher U/Th concentration ratio compared to the Merapi magma (e.g., 0.65 (Handley et al., 2014) relative to 0.22-0.24, respectively, Table 1) and will be older than 380 ka. Carbonate crustal material is therefore, projected to sit on the equiline in Fig. 2 but at higher ($^{238}U/^{232}Th$) and ($^{230}Th/^{232}Th$) than the volcanic samples. Using the U and Th concentrations of local Javanese calcareous sediments (Handley et al., 2014; Fig. 2 caption) and chalky lithic clasts found in the 1883 Krakatau eruption deposits (Gardner et al., 2012) and assuming that ($^{238}U/^{232}Th$) is in secular equilibrium, the local calcareous sedimentary crust would have ($^{238}U/^{232}Th$) (and also therefore, ($^{230}Th/^{232}Th$) ratios) of between 0.85 and 1.98 (Fig. 2). The arrows on Fig. 2a show the expected impact on the activity ratios from the addition of such carbonate material. The 2010 Merapi data are relatively scattered in ($^{238}U/^{232}Th$)-($^{230}Th/^{232}Th$) space and therefore, it is not possible to rule out the influence of carbonate assimilation in the more recent explosive eruption. However, calc-silicate xenoliths were found in the 2006 and 2010 volcanic deposits (e.g., Borisova et al., 2016) and therefore, due to the overlap in U-series isotopic composition of the 2006 and 2010 samples, it is deemed unlikely that a greater amount of carbonate assimilation was implicated in the 2010 eruption based on the U-series data and field observations. The Merapi 2006 and 2010 Sr-Nd-Pb radiogenic isotopic compositions show no difference between eruptions, or in the case of Pb isotopes, with previous eruption periods (Fig. 4a), therefore, again it is considered unlikely that there was a greater degree of carbonate assimilation in 2010 compared to 2006 as a primary explanation for the change in explosivity. Furthermore, in a plot of ($^{230}Th/^{232}Th$) activity ratio versus $^{87}Sr/^{86}Sr$ (Fig. 4b) the 2010 Merapi data show no greater predicted influence from local crustal/carbonate material in magma genesis compared to 2006 and other Javanese volcanic rocks.

As carbonate crustal material will be significantly older than 8000 years (5 times the half-life of ^{226}Ra) it is expected to have ($^{226}Ra/^{230}Th$) = 1, i.e. to be in secular equilibrium. Local limestone/calcareous marl crust is also characterised by significantly lower SiO_2 content compared to the Merapi volcanic rocks (Handley et al., 2014), therefore, bulk assimilation of limestone by magma would lead to a shift to lower SiO_2 and ($^{226}Ra/^{230}Th$). In contrast, addition of fluid produced from skarnification processes would lead to a shift to lower SiO_2 and higher ($^{226}Ra/^{230}Th$), presuming that the fluid/solid partition coefficients for Ra are greater than those for Th for this process. Magmatic recharge would be expected to create a shift to higher ($^{226}Ra/^{230}Th$) at constant or variable SiO_2, depending on the SiO_2 composition of the recharging magma (Fig. 5). Assimilation of older igneous crust (older than 8000 years and therefore, in secular equilibrium) of similar composition to the present day Merapi volcanic rocks, would significantly reduce the ($^{226}Ra/^{230}Th$) of the samples with little change in SiO_2 if completely digested. Partial melting of igneous crust could add siliceous material with ^{226}Ra excesses or deficits depending on the residual mineralogy. These processes may create scatter in data on a ($^{226}Ra/^{230}Th$) versus SiO_2 plot, which may have traditionally been interpreted as a timescale for closed-system differentiation (Fig. 5). Therefore, as recharge and assimilation are both implicated for Merapi, changes in ($^{226}Ra/^{230}Th$) are not likely representative of closed-system evolution timescales as was also found at Lopevi volcano in the Vanuatu arc (Handley et al., 2008). The 2006 and 2010 volcanic rocks appear to display different trends in Fig. 5. The 2006 sample suite shows a near vertical trend with a slight increase in SiO_2 content with decreasing ($^{226}Ra/^{230}Th$), which could be interpreted as magmatic differentiation or recharge/assimilation of older igneous material, and the 2010 suite displays a positive correlation between SiO_2 and ($^{226}Ra/^{230}Th$), which could be attributed to bulk carbonate assimilation (see vectors in Fig. 5). However, these observations are largely dependent on the lowermost ($^{226}Ra/^{230}Th$) sample in each eruption suite as the majority of samples show similar ($^{226}Ra/^{230}Th$) ratios. As the U-Th and radiogenic isotopic ratios show little difference between the 2006 and 2010 eruptions (i.e., pointing to a similar source composition for both), the relatively lower SiO_2 content of the 2010 rocks compared to the 2006 rocks is consistent with a more mafic recharge magma that underwent faster ascent/less stalling in the crust (e.g., Surono et al., 2012; Costa et al., 2013; Nadeau et al., 2013; Preece et al., 2013; Borisova et al., 2016) and that may have mixed with a magma compositionally similar to that erupted in 2006.

5.2. Timing of fluid addition and crystallisation (last fractionation of Ra-Th)

As noted above, the Merapi volcanic rocks all have excess ^{226}Ra, relative to its parent nuclide ^{230}Th (Fig. 2), which in arc rocks is commonly attributed to fluid addition from the subducting slab within the last ~8000 years (e.g., Turner and Hawkesworth, 1997; Turner et al., 2001, 2003, cf. Huang et al., 2008; 2016). At Merapi, there is clear evidence for assimilation of carbonate rocks during differentiation (e.g., Costa et al., 2013; Nadeau et al., 2013; Troll et al., 2013; Borisova et al., 2016). One of these lines of evidence is the presence of abundant calc-silicate xenoliths in Merapi lavas (e.g., Gertisser and Keller, 2003a; Troll et al., 2013). In addition, Merapi whole-rock, grain and in-situ feldspar oxygen isotope data suggest that contamination at shallow levels involves a high δ^{18}O component, such as carbonate crust (Troll et al., 2013; Borisova et al., 2016) rather than a low δ^{18}O component, such as hydrothermal fluid. Thus, we postulate that at least part of the enrichments in Ra observed for Merapi magmas may result from fluid transfer from carbonates included within the magma and in the magma chamber walls as they were transformed into calc-silicates (skarns). This carbonate imprint is likely superimposed upon magma compositions already characterised by ^{226}Ra excess. Published Merapi (^{228}Ra/^{232}Th) ratios lie within error of secular equilibrium (Gauthier and Condomines, 1999) and imply that any Ra enrichment to Merapi magmas occurred >30 years before eruption, due to the short half-life of ^{228}Ra (5.75 yrs).

The plagioclase crystal separates from the 2006 and 2010 samples have (^{238}U/^{232}Th) and (^{230}Th/^{232}Th) ratios that lie within the range displayed by the whole rock ratios (Table 1), suggesting that older recycled crystals do not dominate the plagioclase population (cf. van der Zwan et al., 2013). However, plagioclase phenocrysts from Merapi are noteworthy for the abundance of glass inclusions (e.g., Costa et al., 2013). Thus, the similarity in U-Th nuclide abundances between plagioclase separates and whole rocks likely reflects domination of the U-Th budgets in plagioclase crystals by the inclusions, and we cannot rule out that some plagioclase cores have ages that are long compared to the half life of ^{230}Th. In contrast, plagioclase crystal separates from lavas erupted in both years have similar levels of ^{226}Ra excesses over ^{230}Th (Fig. 2b), which are slightly higher than the whole-rock observed ^{226}Ra excesses. The 2010 dense dome plagioclase sample (M11-01P; Table 2) also has excess ^{210}Pb ((^{210}Pb/^{226}Ra)$_0$ = 1.97). As Pb is more compatible than Ra in plagioclase (e.g., Reagan et al., 2008), the ^{210}Pb excess indicates that some plagioclase in Merapi volcanic rocks grew within decades of eruption. Similar to that observed for highly porphyritic andesites from Mount St. Helens (Reagan et al., 2008) and Arenal (Reagan et al., 2006). This timeframe concurs with

estimated plagioclase growth and residence timescales of <34 years for the 2010 eruption given by Borisova et al. (2016) and largely with timescales of Merapi plagioclase crystal growth of 5 to 310 years determined by van der Zwan et al. (2013).

5.3. Timescales of degassing and magma ascent from ^{210}Po-^{210}Pb-^{226}Ra disequilibria

In contrast to other magmatic systems that exhibit complete, or almost complete, loss of ^{210}Po ($t_{½}$ = 138.4 days) on eruption (e.g., Arenal: Gill et al., 1985, Reagan et al., 2006; Mount St. Helens: Reagan et al., 2008), the 2010 Merapi rocks were variably degassed of ^{210}Po upon eruption (Fig. 3), showing no systematic temporal evolution. The light grey dense inclusion (LGD-Inc) clasts from Stage 2 (M11-28b) and Stage 4 (M11-05) were the least degassed of ^{210}Po on eruption (Table 2). Preece et al. (2016) have suggested that these inclusions represent parts of a plug in the shallow conduit and the initial intrusion into the shallow magma plumbing system prior to eruption. Therefore, the magma forming the inclusions may have stalled at a shallow level and cooled below the blocking temperature for degassing Po for a period that was long enough to allow Po to ingrow via radioactive decay from its nuclide parent prior to eruption. If we assume that these samples would have been fully degassed of Po on ascent before reaching the shallow conduit, i.e. had no initial ^{210}Po, the time to rebuild the observed Po by decay from the parent nuclide would be ~53-74 days before eruption. If these samples had initial (^{210}Po/^{210}Pb) ratios of 0.26-0.31 (Table 2), Po ingrowth calculations would suggest that the plug cooled to below the blocking temperature for degassing Po between 29-56 days before it erupted. Therefore, initial intrusion of magma is estimated to have taken place several weeks to several months prior to the onset of the main eruption period. This time frame largely corresponds to a marked increase in all monitored parameters: ground inflation, earthquake counts and seismic energy release from 20 September 2010, and a significant increase in temperature, CO_2/SO_2 and H_2S/SO_2 ratios, in summit fumaroles from the end of September, which suggested a shift to a deep degassing source, attributed to the influx of new magma (Surono et al., 2012). In contrast to the LGD-Inc sample from Stage 4, the DD samples (M11-27-5 and M11-12) from the same eruptive phase have degassed most, if not all, of their Po at the time of eruption. This suggests that despite prior evidence for rapid ascent of the 2010 dome-forming magma, for example, the lack of amphibole breakdown rims (Costa et al., 2013; Preece et al., 2014) and from microlite textural and compositional analysis (Preece et al., 2014; 2016), the magma was still able to efficiently degas and partition Po into the exsolving gas as it ascended to the surface. Le Cloarec and Gauthier (2003) have shown that gases emitted from previously growing domes

572 at Merapi are strongly depleted in the most volatile isotopes and gas species. The white
573 pumice from the post-climatic phase of the eruption (M11-18, Stage 6) was 83% degassed of
574 ^{210}Po on eruption; less degassed relative to the DD samples from Stage 4. The samples were
575 leached prior to analysis and therefore, it is unlikely that this is due to Po condensing on
576 vesicle walls prior to or during eruption. Instead, it may reflect less efficient degassing by this
577 stage of the eruption related to fast magmatic ascent. This is in agreement with microlite
578 textures in the white pumice that indicate despite some stalling in the conduit at 1.4-2.4 km
579 depth, the magma experienced fast final ascent during this stage (Preece et al., 2016).
580 The variation in $(^{210}Pb/^{226}Ra)_0$ measured in the 2006 and 2010 volcanic rocks is
581 comparable to the full range of $(^{210}Pb/^{226}Ra)_0$ reported by Gauthier and Condomines (1999)
582 for rocks erupted between 1981-1995 at Merapi, with most samples showing deficits of ^{210}Pb
583 relative to ^{226}Ra (Fig. 1). This differs with many other arc volcanoes that display values
584 within analytical error of 1 (Reagan et al., 2017). Equilibrium $(^{210}Pb/^{226}Ra)_0$ values in other
585 arc rocks indicate that the last stage of ^{222}Rn degassing must have occurred over a time period
586 short enough to be undetectable using ^{210}Pb-^{226}Ra disequilibria (~less than two years) prior to
587 eruption. In contrast, excess ^{210}Pb is observed in tephra from the cataclysmic eruption of
588 Mount Pinatubo in 1991 that did not significantly vent gases at the surface prior to eruption,
589 and is attributed to ^{210}Pb accumulation in recharging magma at the base of the dacitic
590 Pinatubo reservoir and subsequent mixing (Kayzar et al., 2009). At Merapi, the ^{210}Pb deficits
591 are consistent with the observed evidence for continuous degassing at fumarole fields and
592 through cracks within the dome at Merapi (Le Cloarec and Gauthier, 2003). However, Ra
593 enrichment (relative to ^{210}Pb) can lead to ^{210}Pb deficits if late-stage fluids derived from
594 carbonate skarnification are added to magmas within decades of eruption. ^{210}Pb-^{226}Ra
595 disequilibria may also be affected by the interaction of magma with sulphide melt and brine,
596 which has been suggested for Merapi (e.g., Le Cloarec and Gauthier, 2003; Nadeau et al.,
597 2013; Preece et al., 2014). However, it would be expected that the transfer of sulphide melt or
598 chloride brine from the recharge mafic magma to the shallower magmatic system should
599 largely produce ^{210}Pb excesses, which are not observed in the rocks.
600 What is clear from the new data is that there is a significant range in $(^{210}Pb/^{226}Ra)_0$
601 within a single eruption at Merapi, therefore, process interpretations based on one sample per
602 eruption/year may not yield sufficient information about the plumbing system and degassing
603 behaviour over decadal timescales (cf. Gauthier and Condomines, 1999). Berlo et al. (2006)
604 also observed variability in $(^{210}Pb/^{226}Ra)_0$ within a single eruption at Mount St. Helens and
605 attributed it to tapping magma from various depths. Mineral and mineral-melt

606 thermobarometry studies on the 2006 and 2010 Merapi samples suggest that for both
607 eruptions, magmatic crystallisation (and inferred storage) occurs over a range of depths, from
608 ~30 km deep to the surface (Costa et al., 2013; Preece et al., 2014). Recent phase equilibrium
609 experiments conducted by Erdman et al. (2016) suggest Merapi's pre-eruptive main reservoir
610 is located at a depth of ≥4.5-9 ± 3 km, which is recharged by a higher temperature magma
611 with a higher melt H_2O content from below. Therefore, it is possible that the variability in
612 $(^{210}Pb/^{226}Ra)_0$ within single eruptions at Merapi is related to variation in magmatic source
613 depth, and mixing of a faster moving, more undegassed, recharging magma with slower
614 moving, shallower, more degassed magma as well as any influence from late-stage carbonate
615 assimilation.
616 The 2006 scoria samples are characterised by deficits of ^{210}Pb, with all samples
617 (except one) lying outside of error of secular equilibrium with no clear evolutionary trend in
618 $(^{210}Pb/^{226}Ra)_0$ (Fig. 1). Assuming the simplest model of efficient (complete) removal of ^{222}Rn
619 with other exsolving gas species (e.g. H_2O, CO_2, SO_2), that the influence of carbonate
620 assimilation is similar for all samples, and a system closed to magmatic recharge (equation 11
621 of Gauthier and Condomines, 1999), the range of ^{210}Pb deficits observed in the 2006 Merapi
622 samples imply approximately 2-4 years (with one sample giving 7 years) of degassing prior
623 to eruption (Table 2). This timeframe compares well with maximum timescale estimates
624 using Fe-Mg gradients in 2006 clinopyroxenes of 2.4-5 years for magma influx into
625 intermediate or shallow depth reservoirs prior to eruption (Costa et al., 2013). The agreement
626 between the two approaches suggests that radon degassing from this shallow reservoir may
627 be the dominant process controlling the ^{210}Pb systematics in Merapi rocks. The first signs of
628 activity for the 2006 eruption were detected by seismic and deformation data in July 2005,
629 which may suggest that the magma may have been degassing while ascending from deeper
630 levels for a year or two before its movement to a shallow level storage region was seismically
631 detected. The previous eruption prior to 2006, occurred 5 years earlier in 2001, so the
632 interpretation of a new influx of magma from a deeper region after 2001 is also compatible
633 with Merapi's eruptive history.
634 Despite differences in initial ^{210}Po between the scoria (S2S M11-28a) and light grey
635 inclusion (LGD-Inc M11-28b) samples erupted during the Stage 2 of the eruption on the 26
636 October, both samples appear to have significantly lower initial ^{210}Pb activities of around 2.3-
637 2.5 dpm/g compared to the other 2010 samples (Fig. 3). This suggests that magma involved
638 in the initial eruption had degassed for longer and either that the magma was sourced from a
639 greater depth and/or travelled more slowly to the surface compared with later stages of the

640 eruption. Microlite textures in the rocks suggest that the eruption intensity and decompression
641 rates were faster for Stage 4 and 6 samples compared to Stage 2 (Preece et al., 2016) and
642 therefore, a slower ascent to the surface is the likely explanation for the lower ^{210}Pb activities
643 in Stage 2 samples. The ^{210}Pb deficit of the LGD-Inc (M11-28b) erupted at the start of the
644 2010 eruption on 26 October can be modelled by 8 years of continuous degassing (equation
645 11 of Gauthier and Condomines, 1999; Table 2) prior to emplacement at shallow levels
646 around a month or two prior to the eruption (calculated from the initial ^{210}Po activity). The
647 explosive activity at the start of the eruption on 26 October was accompanied by significant
648 release of SO_2 (Surono et al., 2012; Fig. 1c) and so, as such a large ^{210}Pb deficit is recorded in
649 the inclusion, it is unlikely that a significant volume of this gas was trapped for an amount of
650 time that was long relative to the half-life of ^{222}Rn in the shallow magma system because the
651 decay of ^{222}Rn would have increased the ^{210}Pb activity.
652 The eruption in 2006 was 4 years prior to 2010, suggesting that magma that formed
653 the light grey material may represent slowly ascending, unerupted magma related to
654 magmatic influx from the 2006 magmatic event, as the ^{210}Pb deficits from the 2006 samples
655 suggest between 2-4 years of degassing prior to eruption, giving a total of 6-8 years of
656 degassing for this material. Between 1 and 4 November 2010 in the main dome-building
657 phase (Stage 3, with samples emplaced in PDC deposits during Stage 4), the three samples
658 analysed show small ^{210}Pb deficits to a small ^{210}Pb excess and lie within error of secular
659 equilibrium. This likely represents the arrival of relatively fast moving magma that did not
660 stall and degas for any significant amount of time since its last stagnation point. The rapid
661 ascent of this relatively undegassed magma triggered a sudden release of gas close to the
662 surface, which caused the massive SO_2 flux during the climactic stage (Fig. 1). This
663 interpretation is consistent with previous petrological studies on minerals and melt inclusion
664 work that suggest the supply of a greater volume of volatile-rich, deeper magma in 2010, that
665 ascended fast with little time to degas (Costa et al., 2013; Preece at al., 2013, 2014). For
666 example, maximum times for magma influx prior to eruption estimated from Fe-Mg gradients
667 in clinopyroxenes give shorter timescales for 2010 compared to the 2006 eruption, of 1.6-2.7
668 years relative to 2.4-5 years, respectively (Costa et al., 2013). The white pumice sample
669 erupted during the latest stages of the climatic phase of 5 November (Stage 6) has a slight
670 ^{210}Pb deficit but lies within error of the Stage 4 samples, also suggesting relatively rapid
671 magmatic ascent. Preece et al. (2014) have shown that clinopyroxene in the white pumice
672 samples crystallised from the deeper levels of the plumbing system, suggesting an increase in
673 deep magma supply at this stage of the eruption. The larger size, lower number density and

equant morphologies of microlites in the white pumice, compared to those in samples from other stages of the eruption, suggest that this magma stalled in the conduit at estimated depths of ~1.4-2.4 km prior to a rapid final ascent to the surface (Preece et al., 2016).

Gauthier and Condomines (1999) (grey diamonds Fig. 1) explained the variation observed in $(^{210}Pb/^{226}Ra)_0$ in rocks erupted between 1981 and 1995 by short periods (<10 years) of closed-system evolution and continuous magmatic degassing. They attributed higher $(^{210}Pb/^{226}Ra)_0$ ratios to reinjections of magma and noted that the higher $(^{210}Pb/^{226}Ra)_0$ ratios coincided with explosive gravitational dome collapses in 1984 and 1992. In this study, the generally higher $(^{210}Pb/^{226}Ra)_0$ observed in samples erupted between 1 to 4 Nov 2010, compared to the more effusive 2006 eruption, supports the model by Gauthier and Condomines (1999) that periods of magmatic recharge are linked to rapid dome extrusion and, ultimately, more explosive eruptions at Merapi and the low/zero initial Po activities in these samples suggest that open-system degassing must have occurred very shortly, in the weeks to months, before eruption.

6. Conclusions

The main conclusions from this study are presented schematically in Fig. 6 and are as follows:

1. The similar U-Th-Ra and Sr-Nd-Pb isotopic ratios presented by the 2006 and 2010 Merapi volcanic rocks, along with the presence of calc-silicate xenoliths in both the 2006 and 2010 eruption deposits, suggest that although carbonate crustal assimilation must have played some role in magmatic evolution for both eruptions it is not a significant contributor to the transition in the volcano's explosive style. Evidence for magmatic recharge and crustal assimilation at Merapi means that U-Th-Ra disequilibria cannot be interpreted using a closed-system evolution timescale model. At present, it is unclear whether Ra excesses are fully attributed to fluid addition from the subducting slab or whether Ra is also added by fluids produced from skarn formation over a timeframe of hundreds to several thousand years prior to eruption (Fig. 6 (A)).
2. The repeated measurement of (^{210}Po) activities for samples collected shortly after eruption reveals that sample MER061406-D was not a juvenile fragment of the 2006 eruption and shows that the juvenile 2006 and 2010 samples were all depleted in ^{210}Po, relative to ^{210}Pb, at the time of eruption but were variably degassed (Fig. 6 (C)). In the 2010 samples, the degree of ^{210}Po degassing is directly related to sample texture

and eruption phase, with the greatest degree of degassing observed in the dense dark dome-building samples erupted during the climatic phase of the eruption (97-100% of ^{210}Po degassed on eruption) and the lowest degree of degassing measured in the light grey inclusions (69-74% of ^{210}Po degassed on eruption) from the initial and earlier phases of the eruption. The light grey inclusion samples are interpreted to represent an initial influx of magma into the shallow plumbing system (Preece et al., 2016). If this is the case, Po ingrowth calculations suggest that the initial intrusion 'plug' cooled through the blocking temperature several weeks to several months before eruption, which is consistent with the marked increase in observed monitoring parameters from 20 September 2010 onwards that suggested influx of new magma from deep.

3. This study shows that there is a wide range in $(^{210}Pb/^{226}Ra)_0$ observed in volcanic deposits from single eruptive episodes at Merapi, which are comparable to the entire range in $(^{210}Pb/^{226}Ra)_0$ ratios for rocks erupted between 1981-1995 (Gauthier and Condomines, 1999). Using a model of complete radon degassing, the ^{210}Pb-^{226}Ra disequilibria can be modelled by ~2-4 years and ~0-3 years of degassing prior to eruption in 2006 and 2010, respectively (Fig. 6 (B)). These timeframes correlate well with maximum timescale estimates from Fe-Mg compositional heterogeneities in clinopyroxene, which suggest 2.4-5 years (2006 eruption) and 1.6-2.7 years (2010 eruption) between magma influx into intermediate/shallow depth reservoirs and eruption (Costa et al., 2013). The agreement in timescales using different approaches suggests that despite the potential impact of crustal assimilation on $(^{210}Pb/^{226}Ra)$ ratios, magmatic degassing and recharge alone can explain ^{210}Pb-^{226}Ra disequilibria in Merapi volcanic rocks. In this context, the ^{210}Pb data suggest that the deeper magma involved in the 2010 eruption began degassing only shortly before eruption (possibly due to its rapid ascent). This interpretation is supported by the lack of amphibole reaction rims in 2010 deposits along with microlite textural and compositional analysis, which suggest minimal storage and relatively rapid movement of the 2010 magma relative to that erupted in 2006 (Preece et al., 2013; 2014; 2016). It also corroborates the work of Gauthier and Condomines (1999), suggesting that periods of magmatic recharge are linked to rapid dome extrusion and ultimately, more explosive eruptions at Merapi. Excess ^{210}Pb relative to ^{226}Ra in plagioclase from the 2006 and 2010 volcanic rocks indicates that part of the plagioclase in Merapi volcanic rocks grew within decades of eruption.

7. Acknowledgements

Peter Wieland and Norman Pearson are thanked for analytical assistance at Macquarie University. John Pallister is thanked for contributing three of our samples. We are grateful to Juan Carlos Afonso for the Matlab code to determine the best-fit ingrowth curves for (^{210}Po). This manuscript has also benefited from three anonymous reviews and editorial handling by Rosemary Hickey-Vargas (Associate Editor) and Marc Norman (Executive Editor). HH is supported by an ARC Future Fellowship FT120100440. This work has been supported by the Natural Environment Research Council (NERC) through Urgency Grant NE/I029927/1. The Sr-Nd and TIMS and MC-ICP-MS U-series isotope data were obtained using instrumentation funded by DEST Systemic Infrastructure Grants, ARC LIEF, NCRIS, industry partners and Macquarie University.

Figure Captions

Figure 1. a) Initial (^{210}Pb/^{226}Ra)$_0$ activity ratios of the 2006 and 2010 Merapi volcanic rocks (this study) compared to the (^{210}Pb/^{226}Ra)$_0$ activity ratios for Merapi volcanic rocks erupted between 1981 to 1995 (Gauthier and Condomines, 1999; grey diamonds). Panels b) and c) show the detailed changes in (^{210}Pb/^{226}Ra)$_0$ activity ratios throughout the 2006 and 2010 eruptions, respectively. COSPEC SO_2 flux measurements for the 2006 eruption (grey circles in panel b are from the Geological Agency Center for Volcanology and Geological Hazard Mitigation (http://www.vsi.esdm.go.id/index.php/gunungapi/data-dasar-gunungapi/542-g-merapi?start=5) and the maximum flux during 1992-2007 (dashed line in b) and mean SO_2 gas flux data for the 2010 eruption are from Surono et al. (2012).

Figure 2. a) (^{238}U/^{232}Th)-(^{230}Th/^{232}Th) equiline diagram for Merapi volcanic rocks and plagioclase separates. Arrows show the expected impact on whole-rock compositions from: i) magmatic recharge (a likely shift to lower (^{230}Th/^{232}Th) relative to differentiated magma), ii) assimilation of older volcanic material in secular equilibrium (with a similar U/Th elemental ratio to the 2006 and 2010 samples) and/or closed system differentiation (shift to higher (^{230}Th/^{232}Th)), and iii) the potential assimilation of crustal carbonate material (a shift towards the equiline but at significantly higher (^{238}U/^{232}Th)). The vector for carbonate assimilation is estimated using the U and Th concentrations of local Javanese calcareous sediments (data given in Handley et al., 2014 and local upper crust samples MX99-1: U: 1.36 ppm, Th: 4.64 ppm; MX99-2: U: 0.72 ppm, Th: 2.56) and assuming that (^{238}U/^{232}Th) is in secular equilibrium. Previously published whole-rock Merapi data (historical and recent (≤ 200 years

776 old) and older) from Gill and Williams (1990), Gauthier and Condomines (1999) and Turner
777 and Foden (2001), Condomines et al. (2005). b) (^{230}Th/^{238}U)-(^{226}Ra/^{230}Th) diagram for
778 Merapi volcanic rocks and plagioclase separates. Previously published whole-rock Merapi
779 data from Gill and Williams (1990), Gauthier and Condomines (1999), and Condomines et al.
780 (2005). The 'older' Merapi data of Condomines et al. (2005) and the Turner and Foden
781 (2001) data were not used in Fig. 2b due to either i) uncertainty in the eruption age of the
782 sample or, ii) samples had assumed, and not measured, (^{230}Th/^{232}Th ratios).
783
784 Figure 3. Plot of ^{210}Po activities versus days since eruption for leached Merapi whole-rock
785 volcanic samples. Note that only two of the 2006 samples were analysed in the days (rather
786 than years) following the eruption. The 2006 sample, MER061406-D, has high initial ^{210}Po
787 and is therefore, not a juvenile fragment of the 2006 eruption. For the 2006 samples that were
788 more than two years old at the time of measurement ('other 2006'), i.e. five times the half-life
789 of ^{210}Po (138.4 days), (^{210}Pb) was considered equal to (^{210}Po) and these samples are plotted
790 on the right-hand y-axis (plotted arbitrarily at 1000 days) for comparison of initial (^{210}Pb)
791 activities. Indicated initial (^{210}Po) and (^{210}Pb) values (Table 2) were obtained through a
792 Markov Chain Monte Carlo simulation using Matlab (see Section 3). Error bars represent 2σ
793 total analytical error. Refer to Table 1 and the text for further eruption framework details and
794 clast type information.
795
796 Figure 4. a) ^{87}Sr/^{86}Sr versus ^{143}Nd/^{144}Nd for the 2006 and 2010 Merapi volcanic rocks.
797 Previously published Merapi data (grey-filled diamonds) from Debaille et al. (2006),
798 Gertisser and Keller (2003a) and Woodhead et al. (2001). Java (including Krakatau) volcanic
799 rock data (grey crosses) from Edwards et al. (1993), Gerbe et al. (1992), Handley et al. (2007:
800 2008; 2010; 2011), Sendjaja et al. (2009), Turner and Foden (2001), Vukadinovic and
801 Sutawidjaja (1995), White and Patchett (1984), Woodhead et al. (2001). Inset shows Pb
802 isotopic ratios for the 2006 and 2010 Merapi volcanic rocks relative to recent high-K (<1900
803 ^{14}C yr B.P.) and medium-K (>1900 ^{14}C yr B.P.) Merapi volcanic rocks (green triangles)
804 (Handley et al., 2014). b) (^{230}Th/^{232}Th) versus ^{87}Sr/^{86}Sr for the 2006 and 2010 Merapi
805 volcanic rocks. The (^{230}Th/^{232}Th) activity ratios for all samples, except the volcanic rock
806 samples from Merapi and Java were calculated using their U and Th concentrations and
807 assuming that (^{238}U/^{232}Th) is in secular equilibrium. Previously published Merapi data from
808 Turner and Foden (2001). Java volcanic rock field (Galunggung and Krakatau) from Turner

and Foden (2001). Java calcareous crustal data and Merapi calc-silicate xenolith data from Gardner et al. (2012), Gertisser and Keller (2003a), Handley et al. (2014). Bulk Java subducted sediment, Bulk Sumatra subducted sediment and Bulk East Sunda subducted sediment from Plank and Langmuir (1998). Indian Ocean sediments (pelagic: I-Pelag and terrigeneous: I- Terrig) from Ben Othman et al. (1989), Gasparon and Varne (1998) and Plank and Langmuir (1998). Sumatran Granitoids divided into I-type (low Sr isotopic ratio and moderate to high Th isotopic ratio) and S-type (high Sr isotopic ratio and low Th isotopic ratio) from Gasparon and Varne (1995). Altered oceanic crust (AOC) lies off the top of the diagram at significantly higher Th isotopic ratios ((^{230}Th/^{232}Th) = 8.78 to 53.4) (Staudigel et al., 1995). Inset diagram shows a close up view of the Merapi and Java volcanic data.

Figure 5. (^{226}Ra/^{230}Th) activity ratio versus SiO_2 (wt%) in Merapi volcanic rocks for the 2006 and 2010 eruptions. SiO_2 contents are taken from Preece et al. (2013) and Preece (2014) and are given in Table 1. Previously published Merapi data are from Condomines et al. (2005). Arrows show the expected impact on whole-rock compositions from: i) magmatic recharge or addition of fluid produced by skarn formation (carb. fluid), ii) assimilation of older volcanic material in secular equilibrium with similar SiO_2 content to the 2006 and 2010 samples and/or closed system differentiation and iii) the potential assimilation of crustal carbonate material (a shift towards secular equilibrium and lower SiO_2 content).

Figure 6. Schematic diagram showing the uranium isotope activity ratios used and the timescales of magmatic processes that have been deduced for the 2006 and 2010 eruptions at Merapi. A: ^{226}Ra and ^{238}U excesses indicate addition of ^{226}Ra on a timescale of 8000 years or less and for ^{238}U on a timescale of <380,000 years, probably due to fluid addition from the subducting slab. It is unconstrained at present whether crustal assimilation of carbonate material or skarn formation processes have added additional ^{226}Ra and ^{238}U to the magma. B: Shallow degassing of ^{222}Rn occurred ~2-4 years prior to eruption in 2006 and ~0-3 years in 2010, suggesting that the ascent of volatile-rich magma shortly before eruption contributed to the greater explosivity observed in 2010. C: Final magma ascent and shallow-level emplacement took place over the weeks to months preceding the eruption as indicated by the degassing of ^{210}Po.

References

842 Allard P. (1983) The origin of hydrogen, carbon, sulphur, nitrogen and rare gases in volcanic
843 exhalations; evidence from isotope geochemistry. In: Tazieff, H. and Sabroux, J. (eds).
844 *Forecasting Volcanic Events*. Elsevier, New York, pp.337–386.
845 Andreastuti S. D., Alloway B. V. and Smith I. E. M. (2000) A detailed tephrostratigraphic
846 framework at Merapi volcano, Central Java, Indonesia: implications for eruption
847 predictions and hazards assessment. *J. Volcanol. Geotherm. Res.***100**, 51-67.
848 Bennett J. T., Krishnaswami I. S., Turekian K. K., Melson W. G. and Hopson C. A. (1982)
849 The uranium and thorium decay series nuclides in Mt. St. Helens effusives. *Earth*
850 *Planet.Sci. Lett.* **60**, 61-69.
851 Ben Othman D. B., White W. M. and Patchett J. (1989) The geochemistry of marine
852 sediments, island arc magma genesis, and crust-mantle recycling. *Earth Planet. Sci.*
853 *Lett.* **94**: 1-21.
854 Berlo K. and Turner S. (2010) ^{210}Pb–^{226}Ra disequilibria in volcanic rocks. *Earth Planet. Sci.*
855 *Lett.* **296**, 155-164.
856 Berlo K., Turner S., Blundy J., Black S. and Hawkesworth C. (2006) Tracing pre-eruptive
857 magma degassing using (^{210}Pb/^{226}Ra) disequilibria in the volcanic deposits of Mount St.
858 Helens. *Earth Planet. Sci. Lett.*, **249**, 337-349.
859 Bourdon B., Ribe N. M., Stracke A., Saal A. E. and Turner S. P. (2006) Insights into the
860 dynamics of mantle plumes from uranium-series geochemistry. *Nature* **444**, 713-717.
861 Birck J. L. (1986) Precision K-Rb-Sr isotope analysis-application to Rb-Sr chronology.
862 *Chem. Geol.* **56**, 73–83.
863 Borisova A. Y., Martel C., Gouy S., Pratomo I., Sumarti S., Toutain J.-P., Bindeman I. N., de
864 Parseval P., Metaxian J.-P. and Surono (2013) Highly explosive 2010 Merapi eruption:
865 Evidence for shallow-level crustal assimilation and hybrid fluid. *J. Volcanol.*
866 *Geotherm. Res.* **261**, 193-208.
867 Borisova A. Y., Gurenko A. A., Martel C., Kouzmanov K., Cathala A., Bohrson W. A.,
868 Pratomo I. and Sumarti S. (2016) Oxygen isotope heterogeneity of arc magma recorded
869 in plagioclase from the 2010 Merapi eruption (Central Java, Indonesia). *Geochim.*
870 *Cosmochim, Acta* **190**, 13-34.
871 Bragagnia A., Avanzinelli R., Freymuth H. and Francalanci L. (2014). Recycling of crystal
872 mush-derived melts and short magma residence times revealed by U-series disequilibria
873 at Stromboli volcano *Earth Planet. Sci. Lett.* 404: 206–219.
874 Camus G., Gourgoud A., Mossand-Berthommier P.-C., and Vincent P.-M. (2000) Merapi
875 (Central Java, Indonesia): An outline of the structural and magmatological evolution,

with special emphasis to the major pyroclastic events. *J. Volcanol. Geotherm. Res.* **100**, 139-163.

Chadwick J. P., Troll V. R., Ginibre C., Morgan D., Gertisser R., Waight T. E. and Davidson J. P. (2007) Carbonate assimilation at Merapi Volcano, Java, Indonesia: Insights from crystal isotope stratigraphy. *J. Petrol.* **48**, 1793-1812.

Charbonnier S.J. and Gertisser R. (2008) Field observations and surface characteristics of pristine block-and-ash flow deposits from the 2006 eruption of Merapi volcano, Java, Indonesia. *J. Volcanol. Geotherm. Res.* **177**, 971-982.

Charbonnier S. J. and Gertisser R. (2011) Deposit architecture and dynamics of the 2006 block-and-ash flows of Merapi Volcano, Java, Indonesia. *Sedimentology* **58**, 1573-1612.

Charbonnier S. J., Germa A. M., Connor C. B., Gertisser R., Preece K., Komorowski J.-C., Lavigne F., Dixon T. H. and Connor L. J. (2013) Evaluation of the impact of the 2010 pyroclastic density currents at Merapi volcano from high-resolution satellite imagery analysis, field investigations and numerical simulations. *J. Volcanol. Geotherm. Res.* **261**, 295-315.

Condomines M., Gauthier P. J., Tanguy J. C., Gertisser R., Thouret J. C., Berthommier P. and Camus G. (2005) ^{226}Ra or ^{226}Ra/Ba dating of Holocene volcanic rocks: application to Mt. Etna and Merapi volcanoes. *Earth Planet. Sci. Lett.* **230**, 289-300.

Condomines M., Gauthier P.-J. and Sigmarsson O. (2003) Timescales of magma chamber processes and dating of young volcanic rocks. In: Bourdon B., Henderson G. M., Lundstrom C. C., Turner, S. P. (Eds.) *Uranium Series Geochemistry*. Reviews in Mineralogy and Geochemistry. The Mineralogical Society of America, Washington, DC, pp. 125–174.

Condomines M., Hemond Ch and Allégre C. J. (1988). U-Th-Ra radioactive disequilibria and magmatic processes. *Earth Planet. Sci. Lett.*, **90**, 243-262.

Condomines M., Sigmarsson O. and Gauthier P. J. (2010) A simple model of ^{222}Rn accumulation leading to ^{210}Pb excesses in volcanic rocks. *Earth Planet. Sci. Lett.* **293**, 331–338.

Costa F., Andreastuti S., de Maisonneuve C. B. and Pallister J. S. (2013) Petrological insights into the storage conditions, and magmatic processes that yielded the centennial 2010 Merapi explosive eruption. *J. Volcanol. Geotherm. Res.* **261**, 209-235.

Cronin S. J., Lube G., Dayudi D. S., Sumarti S., Subrandiyo S. and Surono (2013). Insights into the October–November 2010 Gunung Merapi eruption (Central Java, Indonesia)

910 from the stratigraphy, volume and characteristics of its pyroclastic deposits. *J.*
911 *Volcanol. Geotherm. Res.* **261**, 244–259.
912 Debaille V., Doucelance R., Weis D. and Schiano P. (2006). Multi-stage mixing in
913 subduction zones: Application to Merapi volcano (Java island, Sunda arc). *Geochim*
914 *Cosmochim Acta* **70**, 723–741.
915 Deegan F. M., Troll V. R., Freda C., Misiti V., Chadwick J. P., McLeod C. L. and Davidson
916 J. P. (2010) Magma-carbonate interaction processes and associated CO_2 release at
917 Merapi volcano, Indonesia: insights from experimental petrology. *J. Petrol.* **51**, 1027-
918 1051.
919 Edmonds, M., and Herd R. A. (2007), A volcanic degassing event at the explosive-effusive
920 transition, *Geophys. Res. Lett.*, **34**, L21310.
921 Edwards C. M. H., Morris J. D. and Thirlwall M. F. (1993). Separating mantle from slab
922 signatures in arc lavas using B/Be and radiogenic isotope systematics. *Nature* **362**, 530-
923 533.
924 Erdmann S., Martel C., Pichavant M., Bourdier J.-L., Champallier R., Komorowski J.-C. and
925 Cholik N. (2016). Constraints from Phase Equilibrium Experiments on Pre-eruptive
926 Storage Conditions in Mixed Magma Systems: a Case Study on Crystal-rich Basaltic
927 Andesites from Mount Merapi, Indonesia. *J Petrol* **57**, 535-560.
928 Gardner M. F., Troll V. R., Gamble J. A., Gertisser R., Hart G. L., Ellam R. M., Harris C. and
929 Wolff J. A. (2012). Crustal Differentiation Processes at Krakatau Volcano, Indonesia.
930 *J. Petrol* **54**, 149-182.
931 Gasparon M. and Varne R. (1995). Sumatran granitoids and their relationship to Southeast
932 Asian terranes. *Tectonophysics* **251**, 277–299.
933 Gasparon M. and Varne R. (1998). Crustal assimilation versus subducted sediment input in
934 west Sunda arc volcanics: an evaluation. *Mineral. Petrol.* **64**, 89–117.
935 Gauthier P-J. and Condomines M. (1999). ^{210}Pb-^{226}Ra radioactive disequilibria in recent lavas
936 and radon degassing: inferences on magma chamber dynamics at Stromboli and Merapi
937 volcanoes. *Earth Planet Sci Lett* **172**, 111-126.
938 Gerbe M.-C., Gouraud A., Sigmarsson O., Harmon R.S., Joron J-L. and Provost A. (1992).
939 Mineralogical and geochemical evolution of the 1982-1983 Galunggung eruption
940 (Indonesia). *Bull Volc* **54**, 284-298.
941 Gertisser R., Charbonnier S.J., Keller J. and Quidelleur X. (2012). The geological evolution
942 of Merapi volcano, Central Java, Indonesia. *Bull Volc* **74**, 1213-1233.

943 Gertisser R. and Keller J. (2003a). Trace element and Sr, Nd, Pb and O isotope variations in
944 medium-K and high-K volcanic rocks from Merapi Volcano, Central Java, Indonesia:
945 evidence for the involvement of subducted sediments in Sunda Arc magma genesis. *J.*
946 *Petrol.* **44**, 457–489.
947 Gertisser R. and Keller J. (2003b). Temporal variations in magma composition at Merapi
948 Volcano (Central Java, Indonesia): magmatic cycles during the past 2000 years of
949 explosive activity. *J. Volc. Geotherm. Res.* **123**, 1–23.
950 Gill, J., Williams, R. and Bruland, K. (1985). Eruption of basalt and andesite lava degasses
951 ^{222}Rn and ^{210}Po. *Geophys Res Lett* **12**, 17–20.
952 Gill, J.B. and Williams, R.W. (1990). Th isotope and U-series studies of subduction-related
953 volcanic rocks. *Geochim Cosmochim Acta* **54**, 1427-1442.
954 Handley H.K., Macpherson C.G., Davidson J.P., Berlo K. and Lowry D. (2007) Constraining
955 fluid and sediment contributions to subduction-related magmatism in Indonesia: Ijen
956 Volcanic Complex, Indonesia. *J. Petrol.* **48**, 1155–1183.
957 Handley H.K., Turner S.P., Smith I.E., Stewart R.B. and Cronin S.J. (2008) Rapid timescales
958 of differentiation and evidence for crustal contamination at intra-oceanic arcs:
959 geochemical and U-Th-Ra-Sr-Nd isotopic constraints from Lopevi volcano, Vanuatu,
960 SW Pacific. *Earth Planet. Sci. Lett.* **273**, 184-194.
961 Handley H.K., Macpherson C.G. and Davidson J.P. (2010) Geochemical and Sr–O isotopic
962 constraints on magmatic differentiation at Gede Volcanic Complex, West Java,
963 Indonesia. *Contrib. Mineral. Petrol.* **159**, 885–908.
964 Handley H.K., Turner S., Macpherson C.G., Gertisser R. and Davidson J.P. (2011) Hf–Nd
965 isotope and trace element constraints on subduction inputs at island arcs: Limitations of
966 Hf anomalies as sediment input indicators. *Earth Planet. Sci. Lett.* **304**, 212–223.
967 Handley H.K., Blichert-Toft J., Gertisser R., Macpherson C., Turner S.P., Zaennudin A. and
968 Abdurrachman M. (2014) Insights from Pb and O isotopes into along-arc variations in
969 subduction inputs and crustal assimilation for volcanic rocks in Java, Sunda arc,
970 Indonesia. *Geochim Cosmochim Acta* **139**, 205–226.
971 Hawkesworth C.J., Turner S.P., McDermott F., Peate D.W. and van Calsteren P. (1997) U-Th
972 Isotopes in Arc Magmas: Implications for Element Transfer from the Subducted Crust.
973 *Science* **276**, 551-555.
974 Holden N.E. (1990). Total half-lives for selected nuclides. *Pure Applied Chem* **62**, 941-958.

975 Huang F., Gao L. and Lundstrom C.C. (2008) The effect of assimilation, fractional
976 crystallization, and ageing on U-series disequilibria in subduction zone lavas. *Geochim*
977 *Cosmochim Acta* **72**: 4136–4145.
978 Huang F., Xu J. and Zhang J. (2016) U-series disequilibria in subduction zone lavas:
979 Inherited from subducted slabs or produced by mantle in-growth melting? *Chem Geol*
980 **440**, 179–190.
981 Jeffery A.J., Gertisser R., Troll V.R., Jolis E. M., Dahren B., Harris C., Tindle A.G., Preece
982 K., O'Driscoll B., Humaida H. and Chadwick J.P. (2013). The pre-eruptive magma
983 plumbing system of the 2007–2008 dome-forming eruption of Kelut volcano, East
984 Java, Indonesia. *Contrib. Mineral. Petrol.* **166**, 275-308.
985 Kayzar, T.M., Cooper, K.M., Reagan, M.K. and Kent, A.J.R (2009). Gas transport model for
986 the magmatic system at Mount Pinatubo, Philippines: Insights from (^{210}Pb)/(^{226}Ra). *J.*
987 *Volc. Geotherm. Res*. **181**, 124-140.
988 Komorowski J-C., Jenkins S., Baxter P.J., Picquout A., Lavigne F., Charbonnier S., Gertisser,
989 R., Preece K., Cholik N., Budi-Santoso A. and Surono (2013) Paroxysmal dome
990 explosion during the Merapi 2010 eruption: Processes and facies relationships of
991 associated high-energy pyroclastic density currents. *J. Volc. Geotherm. Res*. **261**, 260-
992 294.
993 Lambert G., Le Cloarec M.F., Ardouin B. and Le Roulley J.C. (1985) Volcanic emission of
994 radionuclides and magma dynamics. *Earth Planet. Sci. Lett.* **76**, 185–192.
995 Le Cloarec M-F and Gauthier P-J (2003). Merapi Volcano, Central Java, Indonesia: A case
996 study of radionuclide behavior in volcanic gases and its implications for magma
997 dynamics at andesitic volcanoes. J Geophys Res **108**, (B5) 2243
998 McDermott F. and Hawkesworth C. (1991) Th, Pb, and Sr isotope variations in young island
999 arc volcanics and oceanic sediments. Earth Planet Sci Lett, **104** 1-15.
1000 Nadeau O., Williams-Jones A.E., Stix J. (2013). Magmatic-hydrothermal evolution and
1001 devolatilization beneath Merapi volcano, Indonesia. *J Volc Geotherm Res* **261**, 50-68.
1002 Newhall C.G., Bronto S., Alloway B., Banks N.G., Bahar I., del Marmol M.A., Hadisantono
1003 R.D., Holcomb R.T., McGeehin J., Miksic J.N., Rubin M., Sayudi S.D., Sukhyar R.,
1004 Andreastuti S., Tilling R.I., Torley R., Trimble D. and Wirakusumah A.D. (2000)
1005 10,000 Years of explosive eruptions of Merapi Volcano, Central Java: archaeological
1006 and modern implications. *J. Volc. Geotherm. Res* **100**, 9-50.

1007 Nguyen, C.T., Gonnermann, H.M., Houghton, B.F. (2014). Explosive to effusive transition
1008 during the largest volcanic eruption of the 20th century (Novarupta 1912, Alaska).
1009 *Geology* **42** (8), 703-706.
1010 Pallister J.S., Schneider D.J., Griswold J.P., Keeler R.H., Burton W.C., Noyles C., Newhall
1011 C.G. and Ratdomopurbo A. (2013). Merapi 2010 eruption - chronology and extrusion
1012 rates monitored with satellite radar and used in eruption forecasting. *J. Volc. Geotherm.*
1013 *Res* **261**, 144-152.
1014 Peate D.W. and Hawkesworth C.J. (2005). U-series disequilibria: insights into mantle
1015 melting and the time scales of magma differentiation. *Rev. Geophys.* **43** RG1003, 1-
1016 43pp.
1017 Pin C. and Zalduegui J.F.S. (1997) Sequential separation of light rare-earth elements, thorium
1018 and uranium by miniaturized extraction chromatography: Application to isotopic
1019 analyses of silicate rocks. *Analytica Chimica Acta* **339**, 79-89.
1020 Plank T. and Langmuir C.H. (1998). The chemical composition of subducting sediment and
1021 its consequences for the crust and mantle. *Chem. Geol.* **145**, 325–394.
1022 Preece K.J. (2014). Transitions between effusive and explosive activity at Merapi volcano,
1023 Indonesia: a volcanological and petrological study of the 2006 and 2010 eruptions.
1024 *Ph.D. Thesis*. University of East Anglia, UK.
1025 Preece K., Barclay J., Gertisser R. and Herd R.A. (2013). Textural and micro-petrological
1026 variations in the eruptive products of the 2006 dome-forming eruption of Merapi
1027 volcano, Indonesia: implications for sub-surface processes. *J. Volc. Geotherm. Res* **261**,
1028 98-120.
1029 Preece K., Gertisser R., Barclay J., Berlo K., Herd R.A. and Edinburgh Ion Microprobe
1030 Facility (2014) Pre- and syn-eruptive degassing and crystallisation processes of the
1031 2010 and 2006 eruptions of Merapi volcano, Indonesia. *Contrib Mineral Petrol* **168**,
1032 1061.
1033 Preece K., Gertisser R., Barclay J., Charbonnier J., Komorowski J.-C. and Herd R.A. (2016)
1034 Transitions between explosive and effusive phases during the cataclysmic 2010
1035 eruption of Merapi volcano, Java, Indonesia. *Bull Volcanol* **78**, 54
1036 Ratdomopurbo A., Beauducel F., Subandriyo J., Agung Nandaka I.G.M., Newhall C.G.,
1037 Suharna Sayudi D.S., Suparwaka H. and Sunarta S (2013) Overview of the 2006
1038 eruption of Mt. Merapi. Journal of Volcanology and Geothermal Research 261: 97-97.

Reagan, M., Tepley III, F.J., Gill, J.B., Wortel, M. and Hartman, B. (2005). Rapid time scales of basalt to andesite differentiation at Anatahan volcano, Mariana Islands. *J. Volc. Geotherm. Res* **146**, 171-183.

Reagan M.K., Tepley III F.J., Gill J.B., Wortel M. and Garrison J. (2006). Timescales of degassing and crystallization implied by ^{210}Po–^{210}Pb–^{226}Ra disequilibria for andesitic lavas erupted from Arenal volcano. *J. Volc. Geotherm. Res* **157**, 135–146.

Reagan, M., Turner S., Handley, H., Turner, M., Beier, C., Caulfield, J. and Peate, D. (2017). ^{210}Pb-^{226}Ra disequilibria in young gas-laden magmas. *Sci. Reports* 7:45186.

Reagan M.K., Cooper K.M., Pallister J.S., Thornber C.R. and Wortel M. (2008). Timing of Degassing and Plagioclase Growth in Lavas Erupted from Mount St. Helens, 2004–2005, from ^{210}Po-^{210}Pb-^{226}Ra Disequilibria. A Volcano Rekindled: The Renewed Eruption of Mount St. Helens, 2004–2006, Edited by David R. Sherrod, William E. Scott, and Peter H. Stauffer *U.S. Geological Survey Professional Paper* **1750**, 847-856.

Reubi O., Sims K.W.W. and Bourdon B. (2014). ^{238}U–^{230}Th equilibrium in arc magmas and implications for the timescales of mantle metasomatism. Earth Planet Sci Lett **391**, 146-158.

Rubin K.H. and Macdougall J. D. (1989) Submarine magma degassing and explosive magmatism at Macdonald (Tamarii) seamount. *Nature* **341**, 50-52.

Rubin K.H. (2001) Analysis of ^{232}Th/^{230}Th in volcanic rocks: A comparison of thermal ionization mass spectrometry and other methodologies. *Chem Geol* **175**, 723-750.

Sendjaja Y.A., Kimura J.-I. and Sunardi E. (2009). Across-arc geochemical variation of Quaternary lavas in West Java, Indonesia: Mass-balance elucidation using arc basalt simulator model. *Island Arc* **18**: 201-224.

Sims K.W.W., Pichat S., Reagan M.K., Kyle P.R., Dulaiova H., Dunbar N.W., Prytulak J., Sawyer G., Layne G.D., Blichert-Toft J., Gauthier P.J., Charette M.A. and Elliott T.R. (2013) On the time scales of magma genesis, melt evolution, crystal growth rates and magma degassing in the Erebus volcano magmatic system using the ^{238}U, ^{235}U and ^{232}Th decay series. J Petrol **54**, 235-271.

Sims K.W.W., Gill J., Dosseto A., Hoffmann D.L., Lundstrom C., Williams R., Ball L., Tollstrup D., Turner S., Prytulak J., Glessner J., Standish J. and Elliott T. (2008). An inter-laboratory assessment of the Th isotopic composition of synthetic and rock standards. *Geostandards Geoanalytical Res* **32**, 65-91.

Staudigel H., Davies G.R., Hart S.R., Marchant K.M. and Smith B.M. (1995). Large scale isotopic Sr, Nd and O isotopic anatomy of altered oceanic crust: DSDP/ODP Sites 417/418. *Earth Planet. Sci. Lett.* **130** 169-185.

Surono, Jousset P., Pallister J., Boichu M., Buongiorno M.F., Budisantoso A., Costa F., Andreastuti S., Prata F., Schneider D., Clarisse L., Humaida H., Sumarti S., Bignami C., Griswold J., Carn S., Oppenheimer C. and Lavigne F. (2012). The 2010 explosive eruption of Java's Merapi volcano - A '100-year' event. *J. Volc. Geotherm. Res.* **241-242**, 121-135.

Troll V.R., Hilton D.R., Jolis E.M., Chadwick J.P., Blythe L.S., Deegan F.M., Schwarzkopf L.M. and Zimmer M. (2012) Crustal CO_2 liberation during the 2006 eruption and earthquake events at Merapi volcano, Indonesia. *Geophys Res Lett* **39**, L11302.

Troll V.R., Deegan F.M., Jolis E.M., Harris C., Chadwick J.P., Gertisser R., Schwarzkopf L.M., Borisova A.Y., Bindeman I.N., Sumarti S. and Preece K. (2013) Magmatic differentiation processes at Merapi volcano: inclusion petrology and oxygen isotopes. *J. Volc. Geotherm. Res.* **261**: 38-49.

Turner S. and Hawkesworth C. (1997). Constraints on flux rates and mantle dynamics beneath island arcs from Tonga–Kermadec lava geochemistry. *Nature* **389**, 568-573.

Turner S., Evans P. and Hawkesworth C. (2001) Ultrafast source-to-surface movement of melt at island arcs from ^{226}Ra-^{230}Th Systematics. *Science* **292**, 1363-1366.

Turner S, Bourdon B and Gill J (2003). Insights into Magma Genesis at Convergent Margins from U-series Isotopes. In: Bourdon, B., Henderson, G.M., Lundstrom, C.C., Turner, S.P. (Eds.), Uranium Series Geochemistry. *Reviews in Mineralogy and Geochemistry*, **52**. The Mineralogical Society of America, Washington, DC, pp. 255-315.

Turner S., Black S. and Berlo K. (2004). ^{210}Pb–^{226}Ra and ^{228}Ra–^{232}Th systematics in young arc lavas: implications for magma degassing and ascent rates. Earth Planet Sci Lett **227**, 1-16.

Turner S.P., George R.M.M., Evans P.J., Hawkesworth C.J. and Zellmer G.F. (2000). Timescales of magma formation, ascent and storage beneath subduction zone volcanoes. *Philos. Trans. R. Soc. Lond.* **358**, 1443–1464.

Turner S., Beier C. Niu Y. and Cook C. (2011).U-Th-Ra disequilibria and the extent of off‐axis volcanism across the East Pacific Rise at 9°30'N, 10°30'N, and 11°20'N, *Geochem. Geophys. Geosyst.* **12**, Q0AC12, doi:10.1029/2010GC003403.

Van der Zwan F.M., Chadwick J.P. and Troll V.R. (2013) Textural history of recent basaltic-andesites and plutonic inclusions from Merapi volcano. *Contrib Mineral Petrol* **166**, 43-63.

Voight B., Constantine E.K., Siswowidjoyo S. and Torley R. (2000). Historical eruptions of Merapi volcano, Central Java, Indonesia, 1768-1998. *J. Volc. Geotherm. Res.* **100**: 69-138.

Vukadinovic D. and Sutawidjaja I. (1995) Geology, mineralogy and magma evolution of Gunung Slamet Volcano, Java, Indonesia. *J Southeast Asian Earth Sci* **11**, 135-164.

Waters C.L., Sims K.W.W., Klein E.M., White S.M., Reagan M.K. and Girard G. (2013) Sill to surface: Linking young off-axis volcanism with subsurface melt at the overlapping spreading center at 9º03'N East Pacific Rise. *Earth Planet. Sci. Lett.* **369-370**, 59-70.

White W. M. and Patchett J. (1984) Hf-Nd-Sr isotopes and incompatible element abundances in island arcs: implications for magma origins and crustal-mantle evolution. *Earth Planet. Sci. Lett.* **67**, 167-185.

Woodhead J.D., Hergt J.M., Davidson J.P. and Eggins S.M. (2001). Hafnium isotope evidence for 'conservative' element mobility during subduction processes. *Earth Planet. Sci. Lett.* **192**, 331–346.

Zobin V.M., Arámbula, R., Bretón, M., Reyes, G., Plascencia, I., Navarro, C., Téllez, A., Campos, A., González, M., León, Z., Martínez, A. and Ramírez, C. (2015). Dynamics of the January 2013–June 2014 explosive-effusive episode in the eruption of Volcán de Colima, México: insights from seismic and video monitoring. *Bull. Volcanol.* 77: 31.

Table 1

Table 1. Uranium-series whole-rock and plagioclase separate data for the 2006 and 2010 Merapi volcanic rocks

Sample Name	Sample Type	Stage	Eruption Age	SiO_2	[U]	±	[Th]	±	$(^{234}U/^{238}U)$	±	$(^{238}U/^{232}Th)$	±	$(^{230}Th/^{232}Th)$	±	$(^{230}Th/^{238}U)$	±
ME08-10	Kali Bebeng Scoria (KB-S)	I	20/05/2006[a]	55.18	1.55	0.04	6.67	0.08	1.003	0.005	0.702	0.006	0.642	0.007	0.914	0.013
M07-53	Lobe 1 - Scoria (L1-S)	II	30/05/2006[b]	55.22	1.50	0.03	6.39	0.08	1.004	0.005	0.712	0.006	0.644	0.007	0.904	0.011
M07-53P	Lobe 1 - Scoria Plagioclase (L1-S-Plag)	II	30/05/2006[b]	n.d.	0.35	0.01	1.51	0.02	1.003	0.005	0.700	0.006	0.640	0.006	0.913	0.010
M07-53P (*rpt*)	Lobe 1 - Scoria Plagioclase (L1-S-Plag)	II	30/05/2006[b]	n.d.	0.35	0.01	1.51	0.02	1.004	0.005	0.703	0.006	0.640	0.006	0.911	0.010
ME08-01	Lobe 4 - Scoria (L4-S)	III	20/06/2006[c]	55.16	1.59	0.04	6.78	0.08	1.002	0.005	0.711	0.006	0.641	0.006	0.901	0.010
ME08-04	Lobe 8 - Scoria (L8-S)	III	20/06/2006[c]	55.40	1.62	0.04	6.94	0.09	1.008	0.005	0.708	0.006	0.638	0.005	0.902	0.009
ME08-07	Lobe 10 - Scoria (L10-S)	III	01/07/2006[c]	55.20	1.49	0.03	6.23	0.08	1.002	0.005	0.720	0.006	0.633	0.005	0.879	0.008
ME08-14	Summit Dome Scoria (SD-S)	IV	01/08/2006[d]	55.47	1.64	0.04	7.06	0.09	1.004	0.005	0.705	0.006	0.640	0.006	0.909	0.011
M11-28b	Light Grey Dense Inclusion (LGD-Inc)	2	26/10/2010	n.d.	1.47	0.03	6.33	0.08	1.006	0.005	0.706	0.006	0.635	0.006	0.899	0.010
M11-05	Light Grey Dense Inclusion (LGD-Inc)	4	01/11/2010[e]	53.76	1.44	0.03	6.49	0.08	1.003	0.005	0.671	0.006	0.636	0.007	0.948	0.013
M11-05 (*rpt*)	Light Grey Dense Inclusion (LGD-Inc)	4	01/11/2010[e]	53.76	1.46	0.03	6.63	0.08	1.003	0.005	0.670	0.006	0.634	0.006	0.946	0.011
M11-12	Dome Dense (DD)	4	01/11/2010[e]	54.77	1.57	0.04	6.64	0.08	1.004	0.005	0.717	0.006	0.627	0.006	0.876	0.010
M11-27-5	Dome Dense (DD)	4	01/11/2010[e]	54.80	1.45	0.03	6.03	0.07	1.004	0.005	0.728	0.006	0.647	0.006	0.889	0.010
M11-01P	Dome Plagioclase (DD-Plag)	4	01/11/2010[e]	n.d.	0.24	0.01	1.03	0.01	1.004	0.005	0.694	0.006	0.641	0.007	0.924	0.012
M11-18	White Pumice (WP)	6	05/11/2010	55.16	1.53	0.03	6.54	0.08	1.002	0.005	0.708	0.006	0.643	0.005	0.908	0.009
TML	Std (Ra)						29.8	0.138					1.070	0.010		
TML	Std (U-Th)				10.7	0.026	29.8	0.081	1.002	0.003	1.090	0.006	1.067	0.007	0.979	0.009
TML	Std (U-Th)				10.9	0.021	30.1	0.064	1.005	0.003	1.097	0.004	1.066	0.005	0.972	0.007
Average TML					10.8		29.9		1.003		1.094		1.068		0.975	
2 Std. Dev.					0.24		0.37		0.005		0.009		0.004		0.009	

Sample Name	Sample Type	Stage	Eruption Age	^{226}Ra (fg/g)	±	$(^{226}Ra/^{230}Th)$	±
ME08-10	Kali Bebeng Scoria (KB-S)	I	20/05/2006[a]	1501	19	3.13	0.12
M07-53	Lobe 1 - Scoria (L1-S)	II	30/05/2006[b]	1474	19	3.19	0.12
M07-53P	Lobe 1 - Scoria Plagioclase (L1-S-Plag)	II	30/05/2006[b]	395	23	3.65	0.22
M07-53P (*rpt*)	Lobe 1 - Scoria Plagioclase (L1-S-Plag)	II	30/05/2006[b]	379	22	3.49	0.21
ME08-01	Lobe 4 - Scoria (L4-S)	III	20/06/2006[c]	1522	19	3.12	0.12
ME08-04	Lobe 8 - Scoria (L8-S)	III	20/06/2006[c]	1517	19	3.05	0.12
ME08-07	Lobe 10 - Scoria (L10-S)	III	01/07/2006[c]	1449	18	3.28	0.12
ME08-14	Summit Dome Scoria (SD-S)	IV	01/08/2006[d]	1398	18	2.76	0.10
M11-28b	Light Grey Dense Inclusion (LGD-Inc)	2	26/10/2010	1378	17	3.06	0.12
M11-05	Light Grey Dense Inclusion (LGD-Inc)	4	01/11/2010[e]	1402	18	3.03	0.11
M11-05 (*rpt*)	Light Grey Dense Inclusion (LGD-Inc)	4	01/11/2010[e]	1390	18	2.95	0.11
M11-12	Dome Dense (DD)	4	01/11/2010[e]	1458	18	3.12	0.12
M11-27-5	Dome Dense (DD)	4	01/11/2010[e]	1396	18	3.19	0.12
M11-01P	Dome Plagioclase (DD-Plag)	4	01/11/2010[e]	258	15	3.49	0.21
M11-18	White Pumice (WP)	6	05/11/2010	1496	19	3.17	0.12
TML	Std (Ra)			3594	26	1.005	0.008

Sample types following Preece (2014) and Preece et al. (2016). SiO_2 (wt %) from Preece et al. (2013) and Preece (2014).
The 2006 eruption stage is taken from Charbonnier and Gertisser (2008) as detailed in Preece et al. (2013). The 2010 eruption stage is taken from Komorowski et al. (2013) as detailed in Preece et al. (2016).
[a]ME08-10 extruded between 1 May and 1 June 2006 and was emplaced between 11 May to 1 June.
[b]M07-53 emplaced in BAFs on 14 June, but extruded between 1st May to 14th June. Microlite textures and lack of amphibole reaction rims in these samples extruded not long before collapse (Preece et al. 2016).
[c]Stage III 2006 samples: extruded post-14 June. Exact date of collapse not know, extrusion between 15 June and early July 2006.
[d]Stage IV 2006 sample: extrusion 15 June - Oct 2006, so an intermediate date in August is assumed for plotting purposes (sample collected in 2008 from the uncollapsed part of the 2006 summit dome).
[e]Samples extruded during Stage 3, between 29 October and 4 November 2010 and emplaced in BAFs and surges on 5 Nov (Stage 4). An intermediate eruption date of 1 November 2010 was used for plotting.
rpt = sample repeat including digestion. n.d. = not determined. Errors on TML are 2SE (measurement precision). Errors given on samples represent 2σ precisions based on TML and sample reproducabilities.

Table 2

Table 2. Measured and initial ^{210}Po and ^{210}Pb activities and ($^{210}Po/^{210}Pb$) and ($^{210}Pb/^{226}Ra$) in Merapi volcanic rock samples

Sample Name	Sample Type	Eruption/ExtrusionDate	Analysis Day	$(^{210}Po)_m$ dpm/g	± 2σ	$(^{210}Po)_i$	± 2σ	$(^{210}Pb)_i$	± 2σ	$(^{210}Po/^{210}Pb)_i$	^{210}Po Degassed (%)	$(^{210}Pb/^{226}Ra)_0$	± 2σ	Years Degassing
MER 95		1995	>700	3.10	0.06			3.05	0.16					
ME08-10	KB-S	20/05/2006	>700	2.96	0.07			2.90	0.09			0.88	0.05	4
ME08-10 (rpt)	KB-S	20/05/2006	>700	2.99	0.07									
M07-53	L1-S	30/05/2006	>700	3.04	0.07			3.01	0.09			0.93	0.06	2
ME08-01	L4-S	20/06/2006	>700	3.03	0.07			2.98	0.09			0.89	0.05	4
ME08-01 (rpt)	L4-S	20/06/2006	>700	3.06	0.07									
ME08-04	L8-S	20/06/2006	>700	2.99	0.07			2.93	0.09			0.88	0.05	4
ME08-04 (rpt)	L8-S	20/06/2006	>700	3.02	0.07									
ME08-07	L10-S	01/07/2006	>700	2.66	0.07			2.57	0.09			0.81	0.06	7
ME08-14	SD-S	01/08/2006	>700	2.95	0.07			2.93	0.09			0.95	0.06	2
MER061406-L	GR-LGS	14/06/2006	37	0.71	0.02	0.21	0.2	3.15	0.10	0.07	93			
			149	1.74	0.04									
			370	2.73	0.05									
			825	3.06	0.06									
MER061406-LL8	leachate	14/06/2006	37	3.81	0.42									
MER061406-D	GR-DGS	14/06/2006	37	2.98	0.05	2.95	0.2	3.12	0.10	0.95				
			149	3.04	0.05									
			370	3.10	0.06									
MER061406-DL8	leachate	14/06/2006	37	2.84	0.32									
M11-28a	S2S	26/10/2010	162	1.62	0.04	0.34	0.20	2.64	0.15	0.13	87			
			475	2.43	0.06									
M11-28b	LGD-Inc	26/10/2010	162	1.60	0.04	0.62	0.20	2.38	0.16	0.26	74	0.79	0.10	8
			475	2.22	0.06									
M11-05	LGD-Inc	1/11/2010	156	2.01	0.05	0.91	0.10	2.93	0.11	0.31	69	0.95	0.07	2
			191	2.15	0.06									
			469	2.71	0.06									
			742	2.90	0.06									
M11-12	DD	1/11/2010	156	1.74	0.05	0.10	0.20	3.11	0.11	0.03	97	0.97	0.07	1
			469	2.76	0.06									
			742	3.08	0.10									
M11-27-5	DD	1/11/2010	156	1.55	0.04	-0.30	0.20	3.13	0.12	-0.10	100	1.02	0.07	0
			469	2.84	0.07									
			891	3.06	0.10									
M11-01P	DD-Plag	1/11/2010	>700	1.12	0.08			1.12	0.10			1.97	0.42	
M11-18	WP	5/11/2010	152	1.85	0.05	0.52	0.20	3.04	0.11	0.17	83	0.92	0.07	3
			465	2.85	0.06									
			738	2.92	0.06									
BCR-2	Rock Standard			1.27	0.04									
BCR-2	Rock Standard			1.24	0.04									

Analysis Day is days after the eruption date. For details on sample eruption date see Table 1. Radium activity is taken from Table 1.
Sample types are given in Table 1. S2S = Pre Nov 5 Scoria; GR-LGS = Gendol River, Light Grey Scoria; GR-DGS = Gendol River, Dark Grey Scoria.
MER061406-D is not a juvenile clast of the 2006 eruption (see text).
MER061406-L was taken from a PDC deposited on 14 June, the exact extrusion age is unknown.
Most 2006 samples were analysed 5-6 years after eruption, which is significantly greater than five times the half-life of ^{210}Po (138.4 days), therefore, (^{210}Pb) was considered equal to measured (^{210}Po) and analysis day is listed as >700 days.
For samples analysed soon after eruption, the initial ^{210}Pb activities, $(^{210}Pb)_i$, representing ^{210}Pb activity at the time of eruption, were calculated using a Matlab code (see text).
The initial ^{210}Pb activities for M11-28a and M11-28b are likely carry greater uncertainty than that shown as they are based on only 2 (^{210}Po) measurements.
The years of magmatic degassing (prior to eruption) is calculated using $(^{210}Pb/^{226}Ra)_0$ and assuming: 1) the simplest model of efficient (complete) removal of ^{222}Rn, 2) that the influence of carbonate assimilation is similar for all samples and, 3) a system closed to magmatic recharge (Equation 11 of Gauthier and Condomines, 1999).
The percentage of ^{210}Po degassed on eruption is calculated using the degassing efficiency factor equation given in Gill et al., 1985.

Table 3

Table 3. Sr, Nd and Pb isotopic data of the 2006 and 2010 Merapi volcanic rocks

Sample	$^{87}Sr/^{86}Sr$	2SE	$^{143}Nd/^{144}Nd$	2SE	$^{206}Pb/^{204}Pb$	$^{207}Pb/^{204}Pb$	$^{208}Pb/^{204}Pb$
M07-53	0.705714	0.000007	0.512718	0.000006	18.762	15.693	39.147
ME08-07					18.766	15.697	39.157
ME08-14					18.762	15.692	39.143
M11-05	0.705742	0.000007	0.512699	0.000008	18.770	15.696	39.162
M11-12	0.705722	0.000006	0.512723	0.000006	18.762	15.694	39.147
M11-18	0.705709	0.000027	0.512711	0.000007	18.762	15.692	39.125
M11-27-5	0.705701	0.000012	0.512718	0.000007	18.760	15.692	39.137
M11-28b	0.705702	0.000009	0.512719	0.000005	18.765	15.697	39.153
SRM 987	0.710214	0.000008					
JMC Nd			0.511116	0.000008			

Pb isotope data are from Handley et al. (2014).

Figure 1

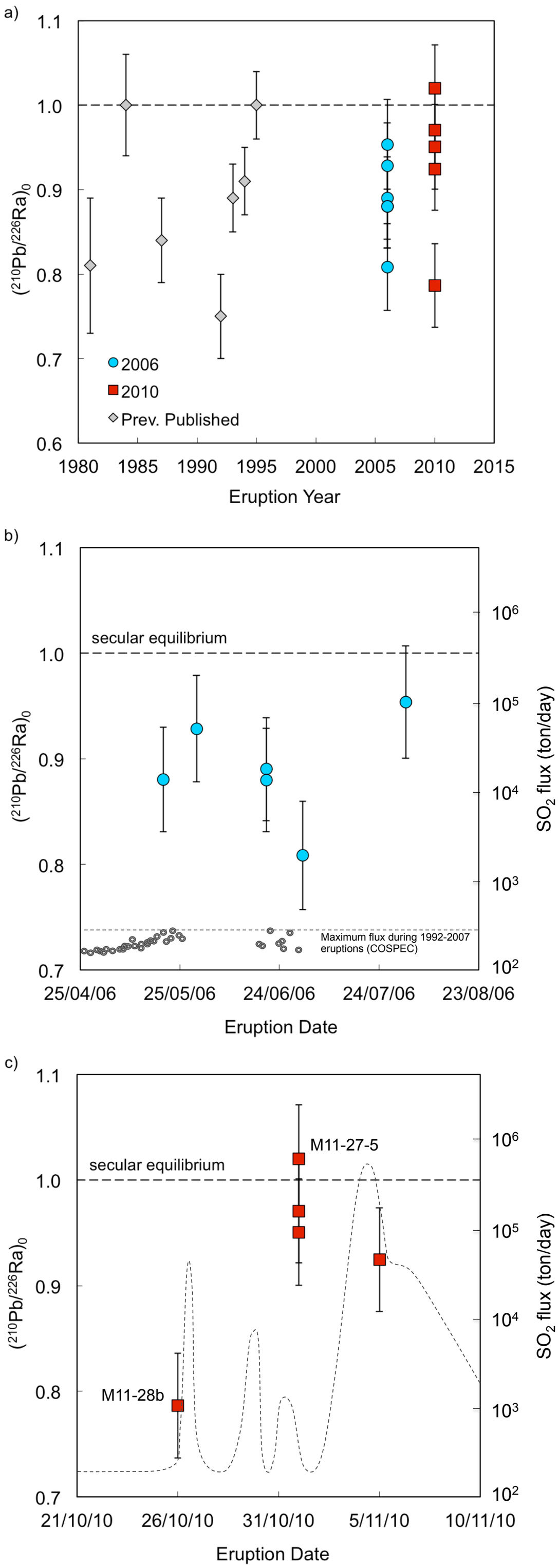
a)
1.1
1.0
0.9
0.8
0.7
0.6
$(^{210}Pb/^{226}Ra)_0$
2006
2010
Prev. Published
1980
1985
1990
1995
2000
2005
2010
2015
Eruption Year
b)
1.1
1.0
0.9
0.8
0.7
secular equilibrium
$(^{210}Pb/^{226}Ra)_0$
10^6
10^5
10^4
10^3
10^2
SO_2 flux (ton/day)
Maximum flux during 1992-2007 eruptions (COSPEC)
25/04/06
25/05/06
24/06/06
24/07/06
23/08/06
Eruption Date
c)
1.1
1.0
0.9
0.8
0.7
secular equilibrium
M11-27-5
M11-28b
$(^{210}Pb/^{226}Ra)_0$
10^6
10^5
10^4
10^3
10^2
SO_2 flux (ton/day)
21/10/10
26/10/10
31/10/10
5/11/10
10/11/10
Eruption Date

Figure 2

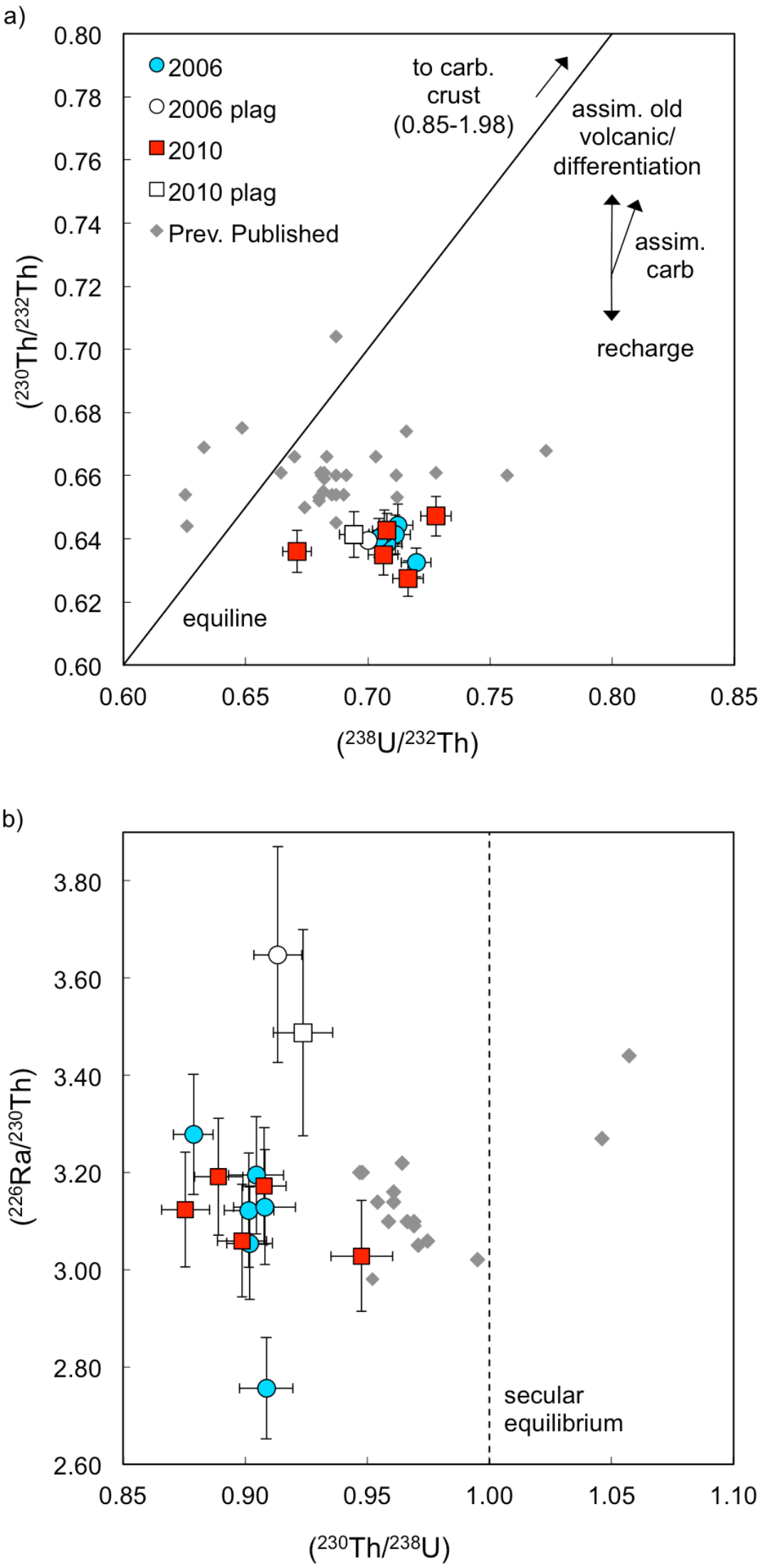
a)
2006
2006 plag
2010
2010 plag
Prev. Published
to carb. crust (0.85-1.98)
assim. old volcanic/ differentiation
assim. carb
recharge
equiline
(230Th/232Th)
(238U/232Th)
0.80
0.78
0.76
0.74
0.72
0.70
0.68
0.66
0.64
0.62
0.60
0.60
0.65
0.70
0.75
0.80
0.85
b)
secular equilibrium
(226Ra/230Th)
(230Th/238U)
3.80
3.60
3.40
3.20
3.00
2.80
2.60
0.85
0.90
0.95
1.00
1.05
1.10

Figure 3

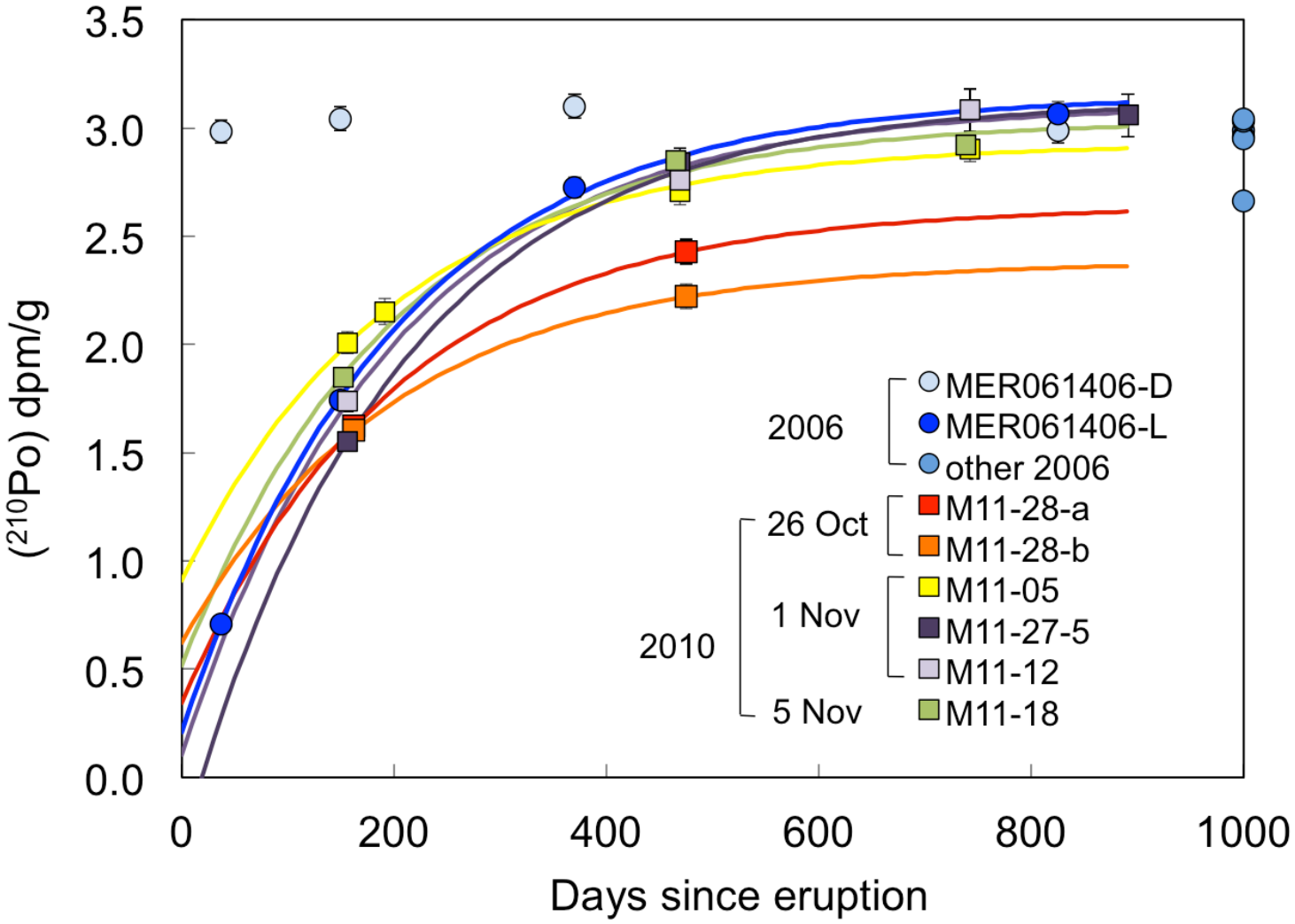
3.5
3.0
2.5
2.0
1.5
1.0
0.5
0.0
(210Po) dpm/g
0
200
400
600
800
1000
Days since eruption
2006
MER061406-D
MER061406-L
other 2006
2010
26 Oct
M11-28-a
M11-28-b
1 Nov
M11-05
M11-27-5
M11-12
5 Nov
M11-18

Figure 4

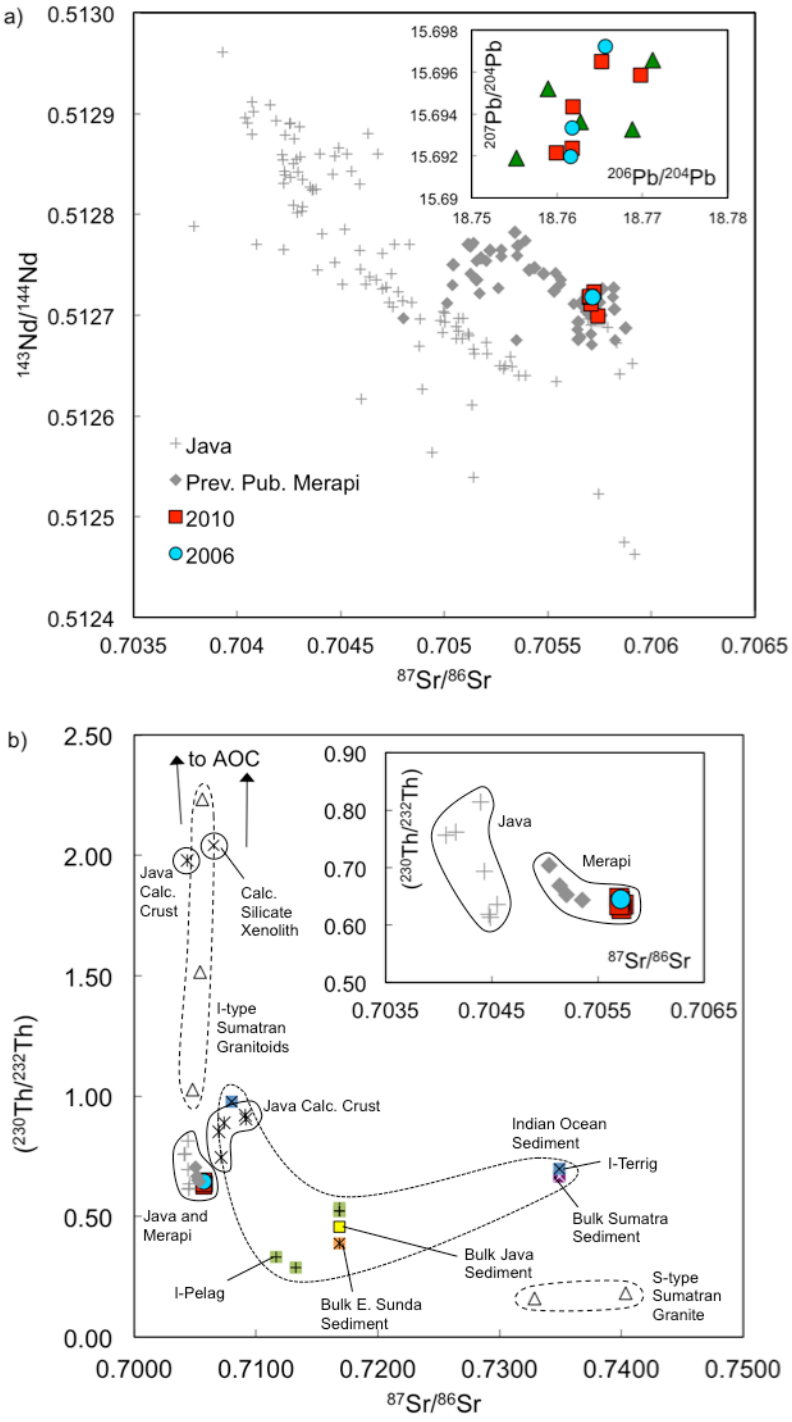
a)
0.5130
0.5129
0.5128
0.5127
0.5126
0.5125
0.5124
143Nd/144Nd
0.7035
0.704
0.7045
0.705
0.7055
0.706
0.7065
87Sr/86Sr
Java
Prev. Pub. Merapi
2010
2006
15.698
15.696
15.694
15.692
15.69
207Pb/204Pb
18.75
18.76
18.77
18.78
206Pb/204Pb
b)
2.50
2.00
1.50
1.00
0.50
0.00
(230Th/232Th)
0.7000
0.7100
0.7200
0.7300
0.7400
0.7500
87Sr/86Sr
to AOC
Java Calc. Crust
Calc. Silicate Xenolith
I-type Sumatran Granitoids
Java Calc. Crust
Java and Merapi
I-Pelag
Bulk E. Sunda Sediment
Bulk Java Sediment
Indian Ocean Sediment
I-Terrig
Bulk Sumatra Sediment
S-type Sumatran Granite
0.90
0.80
0.70
0.60
0.50
(230Th/232Th)
Java
Merapi
0.7035
0.7045
0.7055
0.7065
87Sr/86Sr

Figure 5

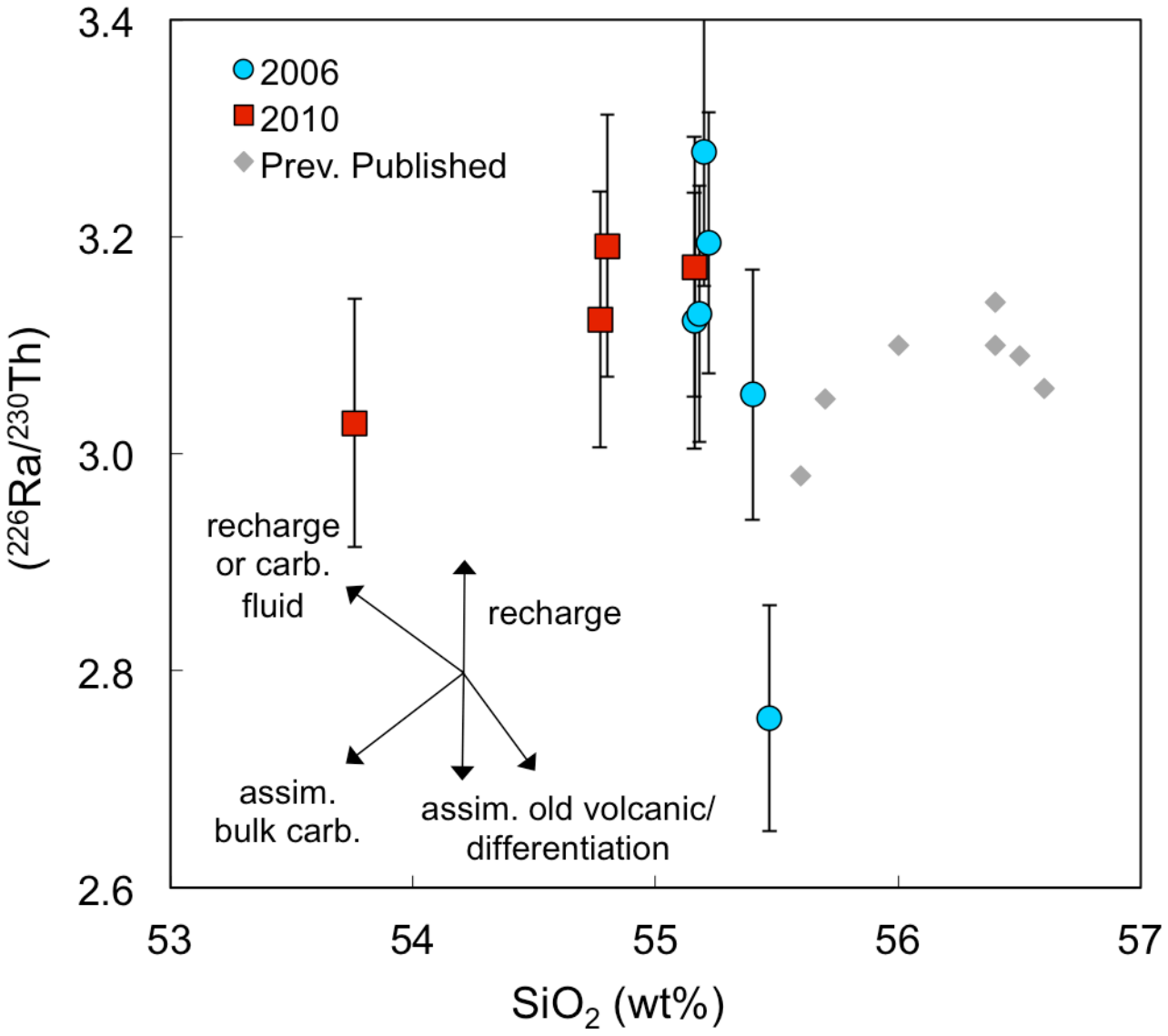
3.4
3.2
3.0
2.8
2.6
53
54
55
56
57
(226Ra/230Th)
SiO2 (wt%)
2006
2010
Prev. Published
recharge or carb. fluid
recharge
assim. bulk carb.
assim. old volcanic/ differentiation

Figure 6

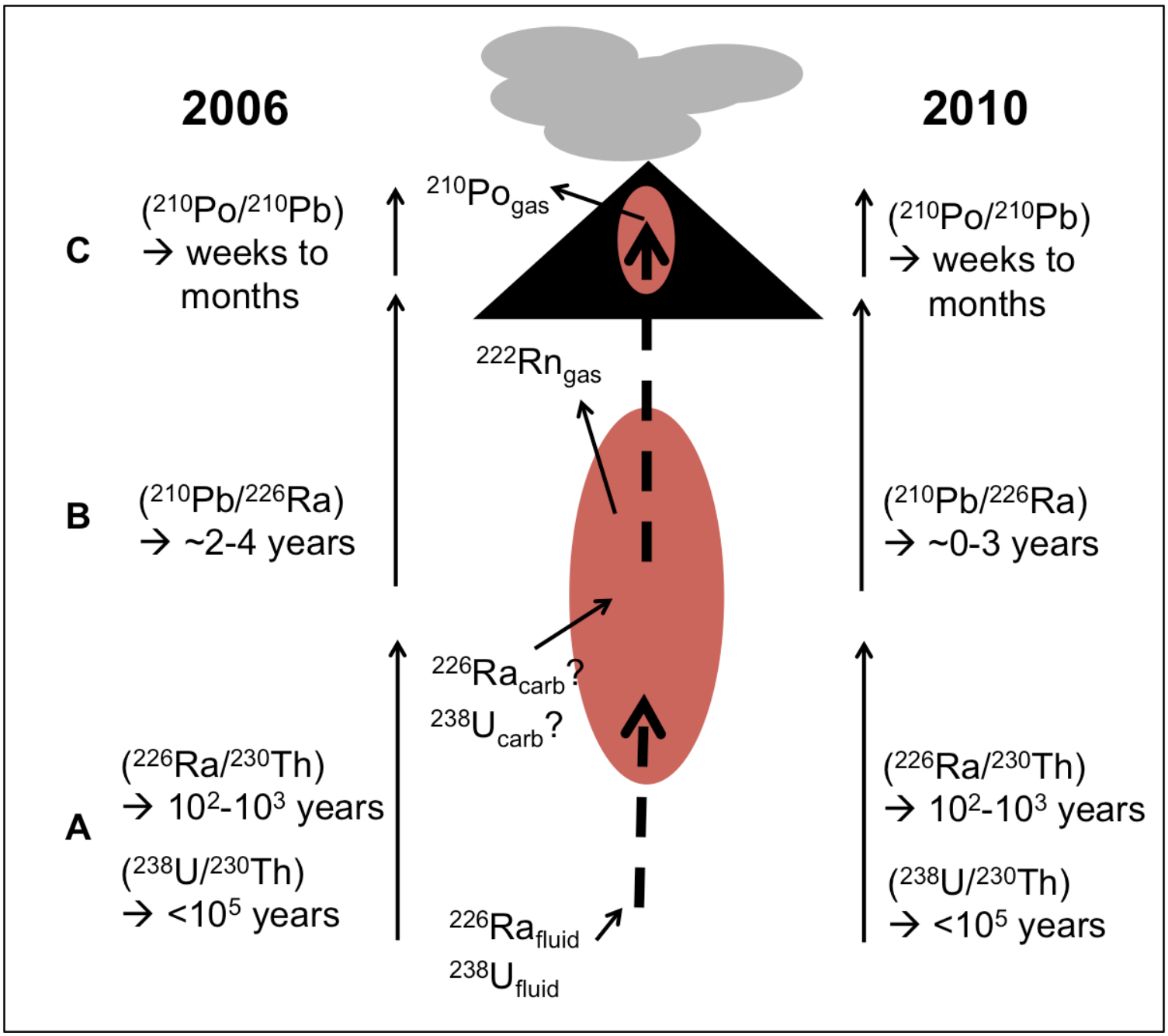
2006
2010
C
(^{210}Po/^{210}Pb)
→ weeks to months
^{210}Po$_{gas}$
(^{210}Po/^{210}Pb)
→ weeks to months
^{222}Rn$_{gas}$
B
(^{210}Pb/^{226}Ra)
→ ~2-4 years
(^{210}Pb/^{226}Ra)
→ ~0-3 years
^{226}Ra$_{carb}$?
^{238}U$_{carb}$?
A
(^{226}Ra/^{230}Th)
→ 10^2-10^3 years
(^{238}U/^{230}Th)
→ <10^5 years
(^{226}Ra/^{230}Th)
→ 10^2-10^3 years
(^{238}U/^{230}Th)
→ <10^5 years
^{226}Ra$_{fluid}$
^{238}U$_{fluid}$